

Pressure Drop and Flow development in the Entrance Region of Micro-Channels with Second Order Velocity Slip Condition and the Requirement for Development Length

Baibhab Ray^{a,*}, Franz Durst^b, Subhashis Ray^{c,*}

^a*Department of Physics, Technische Universität Dresden*

^b*FMP Technology GmbH, Am Weichselgarten 34, 91058 Erlangen, Germany*

^c*Institute of Thermal Engineering, Technische Universität Bergakademie Freiberg
Gustav-Zeuner Straße 7, 09596 Freiberg, Germany*

Abstract

In the present investigation, the development of axial velocity profile, the requirement for development length ($L_{fd}^* = L/D_h$) and the pressure drop in the entrance region of circular and parallel plate micro-channels have been critically analysed for a large range of operating conditions ($10^{-2} \leq Re \leq 10^4$, $10^{-4} \leq Kn \leq 0.2$ and $0 \leq C_2 \leq 0.5$). For this purpose, the conventional Navier-Stokes equations have been numerically solved using the finite volume method on non-staggered grid, while employing the second-order velocity slip condition at the wall with $C_1 = 1$. The results indicate that although the magnitude of local velocity slip at the wall is always greater than that for the fully-developed section, the local wall shear stress, particularly for higher Kn and C_2 , could be considerably lower than its fully-developed value. This effect, which is more prominent for lower Re , significantly affects the local and the fully-developed incremental pressure drop number $K(x)$ and K_{fd} , respectively. As a result, depending upon the operating condition, K_{fd} , as well as $K(x)$, could assume negative values. This never reported observation implies that in the presence of enhanced velocity slip at the wall, the pressure gradient in the developing region could even be less than that in the fully-developed section. From simulated data, it has been observed that both L_{fd}^* and K_{fd} are characterised by the low and the high Re asymptotes, using which, extremely accurate correlations for them have been proposed for

*Corresponding Authors

Email addresses: baibhab.ray@mailbox.tu-dresden.de & baibhab_ray@yahoo.in (Baibhab Ray), f.durst@fmp-technology.com (Franz Durst), ray@iwtt.tu-freiberg.de & juh_p_sray@yahoo.co.in (Subhashis Ray)

both geometries. Although owing to the complex nature, no correlation could be derived for $K(x)$ and an exact knowledge of $K(x)$ is necessary for evaluating the actual pressure drop for a duct length $L^* < L_{fd}^*$, a method has been proposed that provides a conservative estimate of the pressure drop for both $K_{fd} > 0$ and $K_{fd} \leq 0$.

Keywords: Pressure drop, Flow Development, Development length, Pipe and channel flows, Second-order slip boundary condition, Incremental pressure drop number

Contents

Nomenclature	3
1 Introduction and Aim of Work	4
2 Mathematical Formulation	12
2.1 Governing Equations and Boundary Conditions	12
2.2 Analytical Solution for Fully-developed Flow	13
2.3 Numerical Simulations and Post Processing of Data	15
3 Results and Discussion	18
3.1 Development of Velocity Profile	19
3.2 Development Lengths and Correlations	21
3.3 Incremental Pressure Drop Number	26
4 Summary, Conclusions and Final Remarks	39
References	42
List of Figures	52
List of Tables	52

Nomenclature

A_c	Cross-sectional area (m^2)
b	Half gap between two parallel plates (m)
C_1, C_2	First and second order coefficients for wall velocity slip condition
D	Pipe diameter (m)
D_h	Hydraulic diameter = D for pipe and = $4b$ for parallel plate channel (m)
f	Fanning friction factor, $2\tau_w/\rho u_{av}^2$
H	Gap between two parallel plates = $2b$ (m)
k_{ij}	Coefficients in the correlation for K_i
K	Incremental pressure drop number
K_i	Coefficients in the correlation for K_{fd}
Kn	Knudsen number
l_{ij}	Coefficients in the correlation for L_i
L	Axial length (m)
L_i	Coefficients in the correlation for L_{fd}^*
n	Outward normal coordinate from the computational domain (m)
p	Effective pressure (Pa)
P_w	Wetted perimeter (m)
q	Exponent in the correlation for L_{fd}^*
r	Identifier for the coordinate system, also the radial coordinate (m)
R	Radius of the pipe = $D/2$ (m)
Re	Reynolds number, $\rho u_{av} D_h / \mu$
S_{axi}	Special source term for axi-symmetric coordinates
u	Axial velocity (m/s)
v	Radial (for pipe) or transverse (for channel) velocity (m/s)
x	Axial coordinate (m)
y	Radial (for pipe) or transverse (for channel) coordinate (m)

Greek Letters

λ	Mean free path (m)
-----------	--------------------

μ	Dynamic viscosity (Pa s)
ρ	Density (kg/m ³)
σ	Tangential momentum accommodation coefficient
τ	Shear stress (N/m ²)

Subscripts

app	Apparent
av	Average
c	Centre-line
f	Due to friction
fd	Fully-developed
m	Due to change in momentum
s	Slip
t	Tangential direction
w	Pertaining to wall
x	Pertaining to axial coordinate

Superscripts

*	Dimensionless quantity
---	------------------------

1. Introduction and Aim of Work

With the increasing miniaturisation, considerable technological developments have recently been taken place in order to manufacture fluidic systems with channel dimensions in the micro-metre scale, where the overall system dimensions could vary between a few μm to 1 mm (Ho and Tai, 1998; Gad-el-Hak, 1999, 2001; Karniadakis and Beskok, 2002; Karniadakis et al., 2005). As a result, one can easily find numerous examples of micro-channel flows in a broad range of scientific applications and also in everyday use scenarios, such as, the cooling of micro-electronic components and integrated circuits, the gas lubrication in micro-bearings, the active control of aerodynamic flows, the liquid ink flow through the print-heads of ink-jet printers, the extraction of biological samples and the development of micro analysis platforms dubbed “Lab-on-a-chip”, etc., to mention a few

(Barber and Emerson, 2006; Tang et al., 2008).

Owing to its importance in the present context, several articles providing reviews on general and specific topics, monographs and books have been published over the past few decades, emphasising on different aspects of the micro-channel flows. Other than those presenting the broad-based general information, mentioned before, these documents may be classified into the ones specifically dealing with:

1. Predictions of flows using the conventional Navier-Stokes (NS) equations along with different velocity slip and temperature jump conditions at the wall (Arkilic et al., 1997; Karniadakis and Beskok, 2002; Colin, 2005; Karniadakis et al., 2005; Barber and Emerson, 2006; Dongari et al., 2007; Tang et al., 2007a,b; Weng and Chen, 2008; Cao et al., 2009; Chen and Bogy, 2010; Colin, 2012; Zhang et al., 2012b),
2. Modelling of flows employing higher order equations than the conventional NS equations (Hadjiconstantinou, 2000; Jin and Slemrod, 2001; Struchtrup and Torrilhon, 2003; Hadjiconstantinou, 2006; Shan et al., 2006; Ansumali et al., 2007; Lilley and Sader, 2008; Struchtrup and Torrilhon, 2008; Weng and Chen, 2008; Dongari et al., 2009; Roohi and Darbandi, 2009; Dongari et al., 2010),
3. Use of i) kinetic theory of gases (Loyalka, 1971; Cercignani, 1990), ii) Molecular Dynamic (MD) simulations (Bird, 1994; Zhang et al., 2012a), iii) Discrete Simulations Monte Carlo (DSMC) methods (Pan et al., 1999; Hadjiconstantinou, 2000), iv) Non-linear and linearised Boltzmann Equation (BE) (Cercignani, 1975, 1988; Li and Kwok, 2003) and v) Lattice Boltzmann Method (LBM) (Cornubert et al., 1991; Sbragaglia and Succi, 2005; Zheng et al., 2006; Tang et al., 2008; Aidun and Clausen, 2010; Zhang, 2011) for predictions,
4. Effects of compressibility on the flow behaviour and employment of rarefied gas dynamics (Beskok and Karniadakis, 1996; Sharipov and Seleznev, 1998; Cercignani, 2000; Siewert and Sharipov, 2002; Sharipov, 2003; Colin, 2005; Barber and Emerson, 2006; Dongari et al., 2011a,b) for predicting micro-channel flows and
5. Heat transfer enhancement and its characteristics (Gad-el-Hak, 2006; Colin, 2012; Kandlikar et al., 2013) associated with micro-channel flows.

Micro-channel flows are often characterised by the higher mean free path (λ) of the gas molecules that is comparable with the typical system dimension. In this respect, the Knudsen number may be defined as $Kn = \lambda/L_{ref}$, where L_{ref} is the reference or the characteristic length. For the present investigation, L_{ref} for defining Kn has been chosen as the diameter of the capillary D for pipe flows and the gap between two parallel plates $H = 2b$ for channel flows. It appears that Schaaf and Chambre (1961) first proposed the classifications of gas flow regimes based on Kn as:

1. The continuum regime holds for $Kn \leq 10^{-2}$, where both continuum and local thermodynamic equilibrium assumptions are valid and hence the flow is governed by the conventional NS equations with the traditional no-slip condition at the wall.
2. The slip flow regime is identified by $10^{-2} < Kn \leq 10^{-1}$, where the non-equilibrium effects, particularly close to the walls, start dominating the flow and hence the conventional no-slip boundary condition becomes invalid. It is, however, well established that the bulk flow outside the Knudsen layer, whose thickness is estimated to be of the order of λ (Zhang et al., 2006a,b, 2012b), is still governed by the traditional NS equations (Dongari et al., 2007; Karniadakis et al., 2005) and hence the gaseous micro-channel flows in this regime may still be predicted by employing the velocity slip and the temperature jump conditions at the walls, while describing the fluid motion by the continuous NS equations.

Alternatively, as Durst and his co-workers (Chakraborty and Durst, 2007; Dongari et al., 2009, 2010) suggested, the extended NS equations may be invoked for predictions that takes the self diffusion of mass into account. In this formulation, the mass velocity of the fluid is divided into its diffusive and convective parts, where the former explicitly depends on the local gradients of pressure and temperature and produces velocity slip at the wall, while the no-slip boundary condition applies for the convective velocity (Sambasivam, 2013).

The present investigation has been carried out for $Kn \leq 0.2$ and hence it primarily falls into the slip flow regime. Therefore, the conventional NS equations, along with

the velocity slip condition at the wall, have been employed for modelling.

3. The transition regime is characterised by $10^{-1} < Kn \leq 10$, where the rarefaction effects dominate and hence both continuum and local thermodynamic equilibrium assumptions tend to fail. For the early transition regime, however, the predictions obtained using the conventional NS equations require the employment of higher order velocity slip condition at the wall in order to compensate for the non-linear stress-strain relationship and the variation in effective viscosity within the Knudsen layer (Barber and Emerson, 2006; Dongari et al., 2007). Alternatively, costlier methods, like MD simulations, DSMC, or methods derived from the kinetic theory and the BE should be adopted for reliable predictions.
4. The regime beyond $Kn = 10$ is recognised as the free molecular regime, where, owing to the large separation between the gas molecules, the inter-molecular interactions are negligible as compared to the collisions of molecules with the confining walls (Beskok and Karniadakis, 1999; Karniadakis and Beskok, 2002).

While analysing ducted flows, however, it is essential to differentiate the hydro-dynamically fully-developed region¹ from the developing region that is observed close to the entrance. It is, therefore, important to determine the development length L_{fd} , in order to ascertain whether simple analytical solutions could be applied for predicting the flow characteristics. As summarised by Durst et al. (2005), for the developing region, semi-analytical, experimental and numerical methods were adopted in the past.

Semi-analytical solutions in the developing region can be obtained only with considerable simplifying assumptions. By neglecting the axial diffusion of momentum, the boundary layer-type assumptions² are typically invoked for this purpose (Shah and London, 1978). However, the experimental and the numerical investigations showed the existence of *velocity overshoots* close to the duct wall, particularly near the inlet, which proves incompatible with the concept of a boundary layer. Moreover, as Durst et al. (2005) pointed

¹Where analytical solutions for velocity distributions could be obtained for most cases.

²With parabolic axial velocity profile that depends on the local centre-line velocity.

out, the axial diffusion plays an extremely important role in the momentum transfer for low Reynolds number flows, pertinent specifically for micro-channels, and hence it cannot be neglected in this regime. Nevertheless, employing such semi-analytical treatments applicable only for the high Reynolds number regime, L_{fd} could be obtained as:

$$L_{fd}/D_h = C \cdot Re \quad (1)$$

where C is a constant and Re is the Reynolds number.³ Based on several investigations, $C \approx 0.05$ is often cited in the standard text books (see for example, White, 2003; Fox et al., 2010) for pipe flows.

Experimental measurements of L_{fd} are similarly confronted with considerable difficulties. Present levels of uncertainty in the measurement of small difference in the centre-line velocity can produce large errors in determining L_{fd} . This was already reported by Durst et al. (2005), which is also evident from the relatively high scattering of the experimentally determined values of C .

Since the semi-analytical and the experimental methods fail to deliver accurate results for L_{fd} , it is obvious that only a numerical approach would be meaningful. Durst et al. (2005) obtained the following correlations for L_{fd} from their numerical investigations, covering a wide range of Reynolds number ($0.01 \leq Re \leq 4000$):

$$L_{fd}/D_h = [(0.619)^{1.6} + (0.0567 Re)^{1.6}]^{1/1.6} \quad \text{for pipe} \quad (2a)$$

$$L_{fd}/D_h = [(0.3155)^{1.6} + (0.01105 Re)^{1.6}]^{1/1.6} \quad \text{for channel} \quad (2b)$$

For channel flows, Durst et al. (2005) presented their correlation for L_{fd}/H as a function of Re_H . In Eq. (2b), however, $Re = \rho u_{av} D_h / \mu$ is used, which is consistent with the present definition and hence the constants differ from that of the original article.

As far as the developing flow through micro-channels are concerned, in spite of a thorough literature review, the present authors are aware about only two articles by Barber

³Most often defined on the basis of average axial velocity u_{av} and hydraulic diameter D_h .

and Emerson (2001) and Ferrás et al. (2012), where the authors numerically determined L_{fd} , employing the simplified first order velocity slip condition at the wall. While Barber and Emerson (2001) considered flows through both pipes and parallel plate channels for $Re \leq 400$, Ferrás et al. (2012) dealt with only the latter geometry and restricted their study for $Re \leq 100$. In order to define the R and Kn , the hydraulic diameter D_h and the gap between parallel plates $H = 2b$ were chosen as the length scales by Barber and Emerson (2001) and Ferrás et al. (2012), respectively.

It may be noted that for pipe flows, in spite of observing the dependence of L_{fd} on both Re and Kn , Barber and Emerson (2001) recommended the use of correlations from Chen (1973) and Dombrowski et al. (1993) irrespective of Kn , although they were obtained for $Kn = 0$ in the continuum regime. Therefore, the validity of the proposed predictive equations for L_{fd} of pipe flows is questionable, particularly for higher Kn .

For parallel plate channels, Barber and Emerson (2001) and Ferrás et al. (2012) proposed different correlations for L_{fd} , presented in Eqs. (3a) and (3b), respectively:

$$\frac{L_{fd}}{4b} = \frac{0.332}{1 + 0.0271 Re} + \left(\frac{1 + 14.78 C_1 Kn_{Dh}}{1 + 9.78 C_1 Kn_{Dh}} \right) 0.011 Re \quad (3a)$$

$$\frac{L_{fd}}{2b} = \frac{1 + 3.15 (C_1 Kn)^{1.2} + 0.28 (C_1 Kn) Re_H^{0.5}}{1 + 3.82 (C_1 Kn)^{1.5} + 0.018 (C_1 Kn) Re_H} [(0.631)^{1.8} + (0.047 Re_H)^{1.8}]^{1/1.8} \quad (3b)$$

where the symbols $Kn_{Dh} = \lambda/D_h$ and $Re_H = \rho u_{av} H/\mu$ are used, highlighting the difference between the former and the present definitions. In Eq. (3a), the first order velocity slip coefficient is defined as $C_1 = (2 - \sigma)/\sigma$ (Barber and Emerson, 2001), where σ is the tangential momentum accommodation coefficient that varies between 0 and 1 for specular and diffusive reflections, respectively (Wu and Bogy, 2001; Lockerby et al., 2004; Lockerby and Reese, 2008), while for Eq. (3b), $\bar{k}_l = C_1 Kn$ is substituted for consistent representation. Comparison of these correlations clearly reveals the apparent contradictions. Equation (3a) suggests that the low Re ($Re \rightarrow 0$) asymptote is independent of Kn_{Dh} ,⁴ whereas the high Re asymptote ($Re \rightarrow \infty$) is a linear function of Re that explic-

⁴ $L_{fd}^* = 0.332$ is obtained from the first term in Eq. (3a) in this limit.

itly depends on Kn_{Dh} . On the other hand, Eq. (3b) shows that the high Re asymptote is given by $L_{fd}/2b \simeq 0.731Re_H^{1/2}$ and hence is independent of Kn ,⁵ although the low Re asymptote clearly depends on Kn . It is, therefore, evident that the discrepancy in L_{fd} for flows through parallel plate channel must be resolved through systematic investigation.

Although the aforementioned contradicting correlations from Barber and Emerson (2001) in Eq. (3a) and Ferrás et al. (2012) in Eq. (3b) were obtained employing the first order velocity slip boundary condition at the wall,⁶ Dongari et al. (2007) clearly demonstrated that such a simplified approximation fails to explain certain unexpected behaviours, such as the Knudsen (1909) paradox. As a viable alternative, they suggested employing the more general second order velocity slip condition at the wall as:

$$u_{t,w} - u_w = -C_1\lambda \left. \frac{\partial u_t}{\partial n} \right|_w - C_2\lambda^2 \left. \frac{\partial^2 u_t}{\partial n^2} \right|_w \quad (4)$$

where u_w is the velocity of the solid wall, u_t is the fluid velocity tangential to the wall and the suffix w refers to the wall. Further, C_1 and C_2 are first and second order velocity slip coefficients, respectively, while n is the local spatial coordinate, pointing outward from the domain. It is also evident that $C_2 = 0$ was explicitly set by both Barber and Emerson (2001) and Ferrás et al. (2012) and hence their predicted results must be questionable.

Another important observation is that although both Barber and Emerson (2001) and Ferrás et al. (2012) numerically solved the developing flow through circular pipes and parallel plate channels, neither of them reported the variations of pressure drop in the entrance region. However, these data, in the form of incremental pressure drop number $K(x)$ (Shah and London, 1978), should be considered extremely important.

In view of the brief literature review, presented so far, few comments are now in order:

1. In the slip flow and the early transition regimes, the conventional NS equations, originally derived for the continuum regime, could be employed for predictions of

⁵In this regime, $L_{fd}/2H$ is expected to be a linear function of Re_H that depends on Kn .

⁶Where the effects of C_1 and Kn cannot be separately distinguished.

micro-channels flows, as long as the second order velocity slip condition is applied at the wall. Similar to the previous studies (Barber and Emerson, 2001; Ferrás et al., 2012), this modelling approach has been adopted also for the present investigation, which has been conducted for $Kn \leq 0.2$.

2. Extremely insufficient data and no reliable correlation are available for L_{fd} of flow through circular micro-channels. For the parallel plate micro-channels, on the other hand, the available correlations for L_{fd} contradict each other and do not respect either the low or the high Re asymptotes for all Kn .
3. Both previous investigations on L_{fd} were carried out by employing the simplified first order velocity slip condition at the wall that fails to explain the Knudsen (1909) paradox (Dongari et al., 2007). It is, therefore, evident that the more general second order velocity slip condition in Eq. (4) should be adopted, from which, the results for the first order velocity slip condition could be retrieved by setting $C_2 = 0$.
4. The investigation for micro-channel flows should also be accompanied by the associated pressure drop data in the developing region. This information was missing in the previous studies and hence demands for a thorough investigation.

Based on the aforementioned observations, the present investigation has been carried out in order to study the pressure drop and the development of axial velocity profile in the entrance regions of circular and parallel plate micro-channels and to determine L_{fd} for such flows. For this purpose, the conventional NS equations have been employed, along with the second order velocity slip condition at the wall for $10^{-4} \leq Kn \leq 0.2$, while assuming the flow to be steady as well as laminar. Since most of the micro-channel flows operate at low Mach numbers, the compressibility effects have been neglected and hence the fluid has been assumed to be incompressible (Barber and Emerson, 2001). In addition, the fluid has been considered to be Newtonian and the flow as isothermal. Since both density and temperature of the fluid have been assumed to be constants and the viscosity of a Newtonian fluid is a weak function of pressure, its variation in space has been neglected.

The present article has been organised as follows. After this section, presenting a brief introduction, the literature review and the motivation, section 2 deals with the governing

equations, their scaling and the employed boundary conditions. This section also provides analytical solutions for the fully-developed flow through both circular and parallel plate micro-channels with second order velocity slip condition at the wall along with some other relevant characteristics. In addition, a brief description of the numerical method is also outlined for the sake of completeness, along with the post-processing of relevant data. The main results, in the form of development of the axial velocity profile, the variations in L_{fd} , their correlations and the variations in $K(x)$ as well as K_{fd} along with the correlations for the latter are presented in section 3. Finally, the conclusions are reported and the final remarks are made in section 4.

2. Mathematical Formulation

2.1. Governing Equations and Boundary Conditions

The conventional NS equations have been used for modelling the developing flow through micro-channels. In order to express the conservation equations in their non-dimensional forms, all coordinates and lengths have been made dimensionless with respect to D_h , while the velocity components have been normalised using u_{av} . On the other hand, the effective pressure, that also includes the hydrostatic pressure variation, has been scaled with respect to ρu_{av}^2 . As a consequence, the governing mass, axial and transverse (for parallel plate channel) or radial (for pipe) momentum conservation equations are obtained as presented in Eqs. (5), (6) and (7), respectively (Bird et al., 2002; White, 2003; Fox et al., 2010):

$$\frac{\partial u^*}{\partial x^*} + \frac{1}{r^*} \frac{\partial}{\partial y^*} (r^* v^*) = 0 \quad (5)$$

$$\frac{\partial}{\partial x^*} (u^* u^*) + \frac{1}{r^*} \frac{\partial}{\partial y^*} (r^* v^* u^*) = - \frac{\partial p^*}{\partial x^*} + \frac{\partial}{\partial x^*} \left(\mu^* \frac{\partial u^*}{\partial x^*} \right) + \frac{1}{r^*} \frac{\partial}{\partial y^*} \left(\mu^* r^* \frac{\partial u^*}{\partial y^*} \right) \quad (6)$$

$$\frac{\partial}{\partial x^*} (u^* v^*) + \frac{1}{r^*} \frac{\partial}{\partial y^*} (r^* v^* v^*) = - \frac{\partial p^*}{\partial y^*} + \frac{\partial}{\partial x^*} \left(\mu^* \frac{\partial v^*}{\partial x^*} \right) + \frac{1}{r^*} \frac{\partial}{\partial y^*} \left(\mu^* r^* \frac{\partial v^*}{\partial y^*} \right) + S_{axi}^* \quad (7)$$

where $r^* = r/D_h$ is the identifier for the coordinate system that is set to unity and y^* for the Cartesian and the cylindrical axi-symmetric coordinates, respectively. Further in Eqs. (6) and (7), $\mu^* = 1/Re$ is the dimensionless viscosity, where $Re = \rho u_{av} D_h / \mu$ is the Reynolds number defined on the basis of the average axial velocity u_{av} and the hydraulic diameter D_h and $S_{axi}^* = \mu^* v^* / r^{*2}$ in Eq. (7) is the special source term that appears

only for the cylindrical axi-symmetric coordinates (pipe flows) and is set to zero for the Cartesian coordinates (flows through parallel plate channels). For further definitions, the nomenclature section may be referred.

In order to solve Eqs. (5) – (7), the following boundary conditions have been applied:

1. At the inlet, i.e., at $x^* = 0$, the flow has been assumed to be uniform and hence $u^* = u_{av}^* = 1$ and $v^* = 0$ have been set for $0 \leq y^* \leq y_{\max}^*$, where $y_{\max}^* = R^* = 1/2$ for pipes and $y_{\max}^* = b^* = 1/4$ (since $D_h = 4b$) for parallel plate channels.
2. At the exit, i.e., at $x^* = x_{\max}^*$, the axial diffusion terms in Eqs. (6) and (7) have been neglected, i.e., $\partial^2(u^*, v^*)/\partial x^{*2} = 0$ have been set for $0 \leq y^* \leq y_{\max}^*$. This condition is considered less stringent as compared to setting $\partial(u^*, v^*)/\partial x^* = 0$, which may be regarded as a special case.
3. On the line of symmetry (centre-line), i.e., at $y^* = 0$, $\partial u^*/\partial y^* = 0$ and $v^* = 0$ have been set for $0 \leq x^* \leq x_{\max}^*$.
4. On the wall, i.e., at $y^* = 1/2$ for pipes and $y^* = 1/4$ for parallel plate channels, the impermeable condition $v^* = 0$ and the second order velocity slip condition in Eq. (4) have been applied for $0 \leq x^* \leq x_{\max}^*$. Using the dimensionless variables and defining Kn as λ/D and $\lambda/H = \lambda/2b$ for pipes and parallel plate channels, respectively, Eq. (4) may be written for $u_w^* = 0$ in its dimensionless form as:

$$u^* = -C_1 \widetilde{Kn} \frac{\partial u^*}{\partial y^*} \Big|_{y^*=y_{\max}^*} - C_2 \widetilde{Kn}^2 \frac{\partial^2 u^*}{\partial y^{*2}} \Big|_{y^*=y_{\max}^*} \quad (8)$$

where, as the definitions suggest, $\widetilde{Kn} = Kn$ and $\widetilde{Kn} = Kn/2$ have been set for pipes and parallel plate channels, respectively. Fitting a second degree polynomial for u^* close to the wall using the boundary and two interior nodes, located at same x^* , the boundary velocity has been iteratively updated using Eq. (8).

2.2. Analytical Solution for Fully-developed Flow

For fully-developed flows, $\partial u^*/\partial x^* = 0$ and $v^* = 0$ and hence Eqs. (5) and (7) are automatically satisfied. Solving the further simplified form of Eq. (6) using the boundary

conditions at $y^* = 0$ and $y^* = y_{\max}^*$, the axial velocity profiles may be obtained as:

$$u_{fd}^* = \frac{u_{fd}}{u_{av}} = 2 \left[\frac{1 - (r/R)^2 + 4C_1Kn + 8C_2Kn^2}{1 + 8C_1Kn + 16C_2Kn^2} \right] \quad \text{for pipe} \quad (9a)$$

$$= \frac{3}{2} \left[\frac{1 - (y/b)^2 + 4C_1Kn + 8C_2Kn^2}{1 + 6C_1Kn + 12C_2Kn^2} \right] \quad \text{for channel} \quad (9b)$$

The slip velocity at the wall $u_{s,fd}^*$ and the centre-line velocity $u_{c,fd}^*$ for fully-developed flows may now be easily retrieved from Eq. (9) by setting $r = R$ or $y = b$ and $r = 0$ or $y = 0$ for pipe or channel flows, respectively. The variations in $u_{s,fd}^*$ and $u_{c,fd}^*$ as functions of Kn are presented in Fig. 1 for different C_2 . The figure shows that $u_{s,fd}^*$ increases and in order to maintain the same dimensionless mass flow rate ($u_{av}^* = 1$), $u_{c,fd}^*$ decreases with the increase in both Kn and C_2 . These variations for different C_2 are also more prominent for $Kn \geq 0.01$, which indicates that the difference between the first and the second order velocity slip conditions at the wall are expected to be more significant for higher Kn and justifies the present investigation. For developing flows, on the other hand, owing to the higher axial velocity gradients at the wall, particularly close to the entrance, the effects of C_2 are expected to be more prominent even at lower Kn .

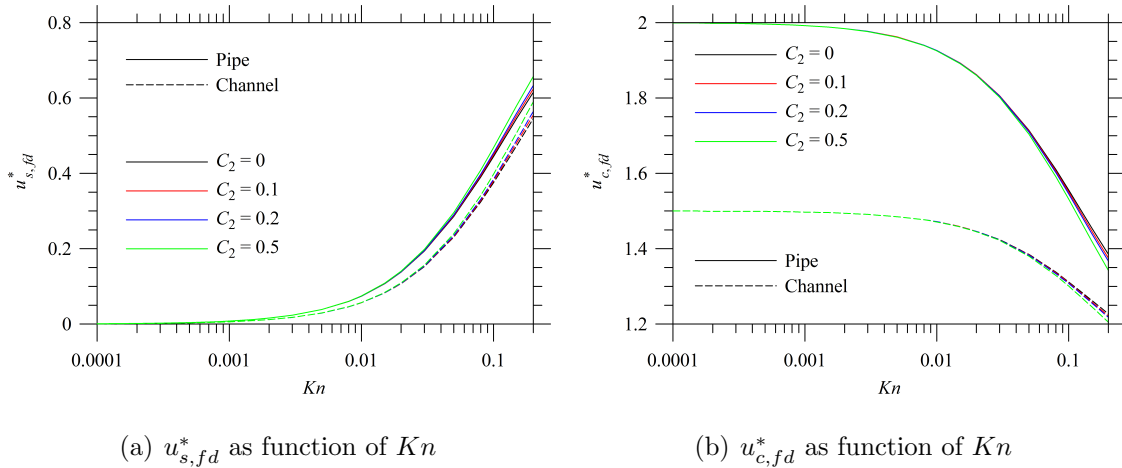


Figure 1: $u_{s,fd}^*$ and $u_{c,fd}^*$ for pipe and channel flows as functions of Kn for different C_2 .

The Fanning friction factor is defined as $f = 2\tau_w/\rho u_{av}^2$ (Shah and London, 1978), where

τ_w as the wall shear stress, and $f_{fd}Re$ may be obtained from Eq. (9) as:

$$f_{fd}Re = \frac{16}{1 + 8C_1Kn + 16C_2Kn^2} \quad \text{for pipe} \quad (10a)$$

$$= \frac{24}{1 + 6C_1Kn + 12C_2Kn^2} \quad \text{for channel} \quad (10b)$$

In the fully-developed section, owing to the absence of inertia (convection) and axial diffusion, the integral force balance could be obtained as $\Delta p_{fd}A_c = \tau_{w,fd}P_w x$, where $\Delta p_{fd} = (-dp/dx)x$ is the pressure drop in the fully-developed section over an axial length x . This relation may be expressed in dimensionless form as $\Delta p_{fd}^* = 2f_{fd}x^*$.

2.3. Numerical Simulations and Post Processing of Data

The numerical code, used by Durst et al. (2005), has been employed also for the present study by modifying the wall boundary condition according to Eq. (8). For this purpose, Eqs. (5) – (7) have been discretised for a given non-staggered control volume (CV) using the finite volume approach (Ferziger and Perić, 1999), where the cell-face velocities have been evaluated using the momentum interpolation method (Rhie and Chow, 1983). The central differencing scheme has been used for both convective and diffusive terms, where the deferred correction approach has been used for the former (Khosla and Rubin, 1974).

The set of discretised equations for a given equation have been solved iteratively by employing the Strongly Implicit Procedure (Stone, 1968), while the SIMPLE algorithm (Patankar and Spalding, 1972; Patankar, 1980) has been used in order to ensure the pressure-velocity coupling. After each iteration, the L2 norms of the residues for all conservation equations have been calculated and the solution has been accepted as converged when all these norms have been found to be less than 10^{-7} .

From the converged solutions, the local friction factors have been obtained as $f_x = 2\tau_{w,x}/\rho u_{av}^2$, where $\tau_{w,x} = \mu(\partial u/\partial y)_{y=y_{\max}}$ is the wall shear stress at x . Using the dimensionless variables and the expression for $\tau_{w,x}$, one obtains:

$$f_x Re = 2 \left. \frac{\partial u^*}{\partial y^*} \right|_{y^*=y_{\max}^*} \quad (11)$$

Durst et al. (2005) pointed out that the flow develops much faster (i.e., at least distance from the entrance) close to the wall as compared to the centre-line. This observation has been found to be true also for the present investigation, irrespective of C_2 , Kn and Re . Therefore, L_{fd} has been always determined by the linear interpolation using two successive nodal velocities between which the centre-line velocity equals 99% of the analytical fully-developed value in Eq. (9).

Alternatively, the length required for $f_x Re$ in Eq. (11) to differ by 1% from $f_{fd} Re$ in Eq. (10) could also be considered as a measure of L_{fd} . As expected, however, since the development of velocity gradient at the wall depends directly on the flow development close to the wall, $f_x Re$ also develops much faster than the centre-line velocity. Therefore, L_{fd} , calculated on the basis of centre-line velocity, provides the most conservative estimate and hence has been adopted for the present investigation.

In order to quantify the pressure drop in the developing region, $K(x)$, according to (Shah and London, 1978), has been evaluated. Assuming a uniform velocity profile at the inlet ($u = u_{av}$) and integrating the dimensional form of Eq. (6), one obtains:

$$\Delta p_x A_c = (p_0 - p_x) A_c = \int_0^x \tau_{w,x} P_w dx + \int_{A_c} \rho u^2 dA_c - \rho u_{av}^2 A_c \quad (12)$$

where p_0 and p_x are the cross-sectional averaged pressure at the inlet and x , respectively:

$$p_0 = \frac{1}{A_c} \int_{A_c} p(0, y) dA_c; \quad p_x = \frac{1}{A_c} \int_{A_c} p(x, y) dA_c; \quad dA_c = r dy \quad (13)$$

In the expression for dA_c in Eq. (13), r has the similar meaning as in Eqs. (5) – (7) with respect to the coordinate system. Dividing Eq. (12) by the inlet momentum $\rho u_{av}^2 A_c$, one obtains Δp_x^* as:

$$\Delta p_x^* = 2 \int_0^{x^*} f_x dx^* + \frac{1}{A_c^*} \int_{A_c^*} (u^*)^2 dA_c^* - 1 = \Delta p_{f,x}^* + \Delta p_{m,x}^* \quad (14)$$

Equation (14) clearly shows that the pressure drop occurs in the axial direction in order to 1) overcome the frictional resistance at the wall (the first term, $\Delta p_{f,x}^*$) and 2) increase the total momentum of the fluid (the last two terms, $\Delta p_{m,x}^*$). For the fully-developed flows

($x \rightarrow \infty$), since the velocity distribution is given by Eq. (9), $\Delta p_{m,\infty}^*$ could be analytically obtained as presented in Eqs. (15a) and (15b) for pipe and channel flows, respectively:

$$\Delta p_{m,\infty}^* = \frac{4[1/3 + (1 + 4C_1Kn + 8C_2Kn^2)(4C_1Kn + 8C_2Kn^2)]}{(1 + 8C_1Kn + 16C_2Kn^2)^2} - 1 \quad (15a)$$

$$= \frac{9[1/5 + (1 + 4C_1Kn + 8C_2Kn^2)(1/3 + 4C_1Kn + 8C_2Kn^2)]}{4(1 + 6C_1Kn + 12C_2Kn^2)^2} - 1 \quad (15b)$$

Like the fully-developed velocity profiles in Eq. (9), $\Delta p_{m,\infty}^*$ is also independent of Re . For $Kn = 0$ (no-slip condition), $\Delta p_{m,\infty}^*$ is obtained as 1/3 and 1/5 for pipe and channel flows, respectively. The variations in $\Delta p_{m,\infty}^*$ as functions of Kn for different C_2 are presented in Fig. 2, which shows $\Delta p_{m,\infty}^*$ decreases rapidly with the increase in Kn , particularly for $Kn \geq 0.01$. Like u_s^* and u_c^* in Fig. 1, the variations are clearly more sensitive on Kn than on C_2 for the investigated ranges.

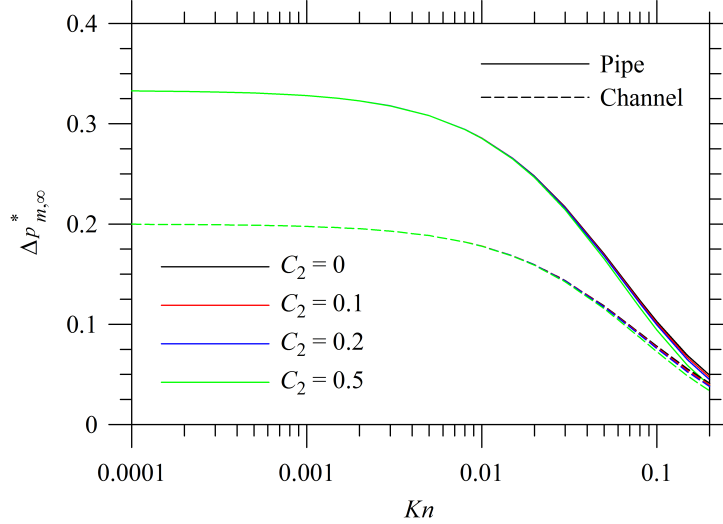


Figure 2: Variations in $\Delta p_{m,\infty}^*$ as functions of Kn for pipe and channel flows.

Similar to f_{fd} in the fully-developed region, the apparent friction factor $f_{app,x}$ may be defined according to $\Delta p_x^* = 2f_{app,x}x^*$. Using this relation and Eq. (14), one obtains:

$$f_{app,x} = \frac{\Delta p_x^*}{2x^*} = \frac{1}{x^*} \left[\int_0^{x^*} f_x dx^* + \frac{1}{2} \left(\frac{1}{A_c^*} \int_{A_c^*} (u^*)^2 dA_c^* - 1 \right) \right] \quad (16)$$

If the flow is assumed to be fully-developed even in the developing region, the pressure drop would be obtained as $\Delta p_{fd}^* = 2f_{fd}x^*$. The incremental pressure drop number $K(x)$

is defined as the difference between the true and the expected fully-developed pressure drops, normalised with respect to $\rho u_{av}^2/2$:

$$\begin{aligned} K(x) &= \frac{2}{\rho u_{av}^2} (\Delta p_x - \Delta p_{fd}) = 2 (\Delta p_x^* - \Delta p_{fd}^*) \\ &= 2 (\Delta p_{f,x}^* + \Delta p_{m,x}^* - 2f_{fd}x^*) \end{aligned} \quad (17)$$

Since $\tau_{w,x}$ is expected to be higher than $\tau_{w,fd}$, Δp_x is also expected to be higher than Δp_{fd} for the same axial distance and hence $K(x)$, irrespective of the operating condition, is expected to be always positive. The present authors are unaware about any case where $K(x)$ has been reported to be negative. Nevertheless, once $K(x)$ is known, Δp_x may be evaluated as:

$$\Delta p_x = \frac{1}{2} \rho u_{av}^2 [K(x) + 4f_{fd}x^*] \quad (18)$$

Unlike $f_{app,x}$, as $x \rightarrow \infty$, $K(x)$ asymptotically assumes a constant value that strongly depends on Re , Kn and C_2 and is denoted as K_{fd} . It is evident that when the length of the duct $L \geq L_{fd}$, K_{fd} plays a direct as well as important role in the calculation of true pressure drop Δp_L and hence the variation in $K(x)$ is considered more important than $f_{app,x}$ in order to characterise the pressure drop in the developing region.

3. Results and Discussion

In the present investigation, numerical simulations have been performed for both pipe and channel flows by varying Re over a wide range from 10^{-2} (diffusion dominated regime) to 10^4 (convective regime), although the micro-channel flows may never encounter a case with extremely high Reynolds number. However, as will be shortly apparent, accurate low and high Re asymptotes are required in order to obtain reliable correlations for L_{fd}^* even in the moderate Re range of practical interest $1 \leq Re \leq 100$ (Barber and Emerson, 2001; Ferrás et al., 2012). For each Re , Kn has been varied from 10^{-4} (continuum regime) to 0.2 (early transition regime). As indicated by Dongari et al. (2007) and Zhang et al. (2012b), most theoretical and experimental studies reported $C_1 \approx 1$, while C_2 varies over a wide range. As a result, for the present investigation, $C_1 = 1$ (special case for $\sigma = 1$) has been chosen, while C_2 has been varied from 0 (first order) to 0.5. The results of Durst

et al. (2005) have been reproduced by setting $Kn = 0$.

Prior to obtaining the results, however, a careful grid independence study has been carried out and x_{\max}^* has been determined in order to ensure that the fully-developed flow condition for a given Re is always satisfied well inside the chosen duct length, irrespective of Kn and C_2 . A preliminary investigation has revealed that other than pipe flows for high Re , L_{fd}^* always increases with the increase in Kn and C_2 . For the most critical case with $C_2 = 0.5$ and $Kn = 0.2$, L_{fd}^* has been observed to be approximately 1.5 to 2 times of that calculated from Eq. (2) for the continuum regime. Therefore, x_{\max}^* for all investigated cases has been specified as 3 times of L_{fd}^* for $Kn = 0$.

The computational domain has been discretised using non-uniform CVs, expanding in the axial direction and contracting in the transverse or the radial direction in geometric progression with common ratios 1.02 and 1/1.02, respectively. The grid independence study showed 300 CVs are required in order to resolve the axial direction, while for the transverse or the radial direction, 80 CVs have been found to be sufficient as far as the evaluation of L_{fd}^* is concerned. The detailed results of the grid independence study, however, are not presented here for brevity.

Unless absolutely required, the results for pipe flows are only presented in this article in order to demonstrate and explain various physical aspects of micro-channel flows, while similar data for parallel plate channels are not presented here for the sake of brevity.

3.1. Development of Velocity Profile

The fully-developed velocity profile in Eq. (9) still remains parabolic, even in the presence of velocity slip at the wall. For no-slip condition at the wall, Durst et al. (2005) already reported that owing to the higher velocity gradient, velocity overshoots occur close to the wall, particularly near the entrance, which subsequently decays and finally disappears. Barber and Emerson (2001) and Ferrás et al. (2012) also observed similar velocity overshoots with the first order velocity slip condition and hence it would be worthwhile

exploring if (and how) this behaviour changes for the second order velocity slip condition.

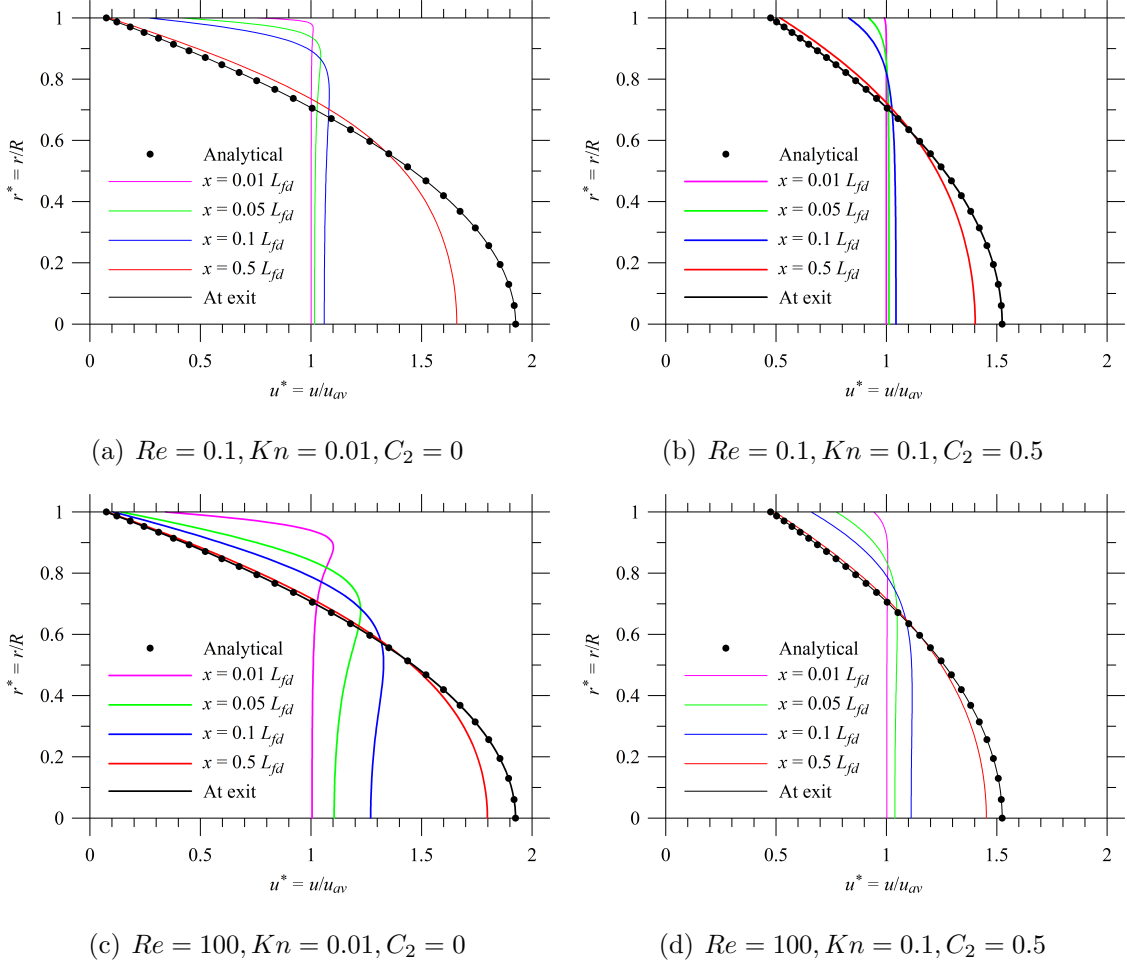


Figure 3: Development of u/u_{av} as functions of r/R at different axial locations for pipe flows.

The velocity profiles at different axial locations are presented in Fig. 3 for pipe flows with $Re = 0.1$ and 100 for $Kn = 0.01$ with $C_2 = 0$ and $Kn = 0.1$ with $C_2 = 0.5$. The figure shows that irrespective of the chosen parameters, the analytical solutions for the fully-developed flows have always been achieved at the exit that justify the present choice of x_{\max}^* . In addition, the velocity overshoot is observed to be more pronounced for higher Re , although even in this regime, it decreases considerably with the increase in both Kn and C_2 . Accordingly, the largest velocity overshoot occurs for the highest Re with $C_2 = 0$ and $Kn = 0$, although the results are not presented in here for brevity. For higher Kn

with $C_2 = 0.5$, the velocity overshoots could be so minute that it may hardly be noticeable.

From the variations of axial velocity profiles in Fig 3, it may appear that the parabolic (quadratic) velocity profile, without any velocity overshoot, could be assumed at least for higher Kn and C_2 and the boundary layer theory could be applied for the prediction. However, similar to $Kn = 0$, such an apprehension could be true only for $Re \rightarrow \infty$ since the effects of axial diffusion are always neglected in such analysis and hence relations similar to Eq. (1) could be retrieved only in the convection dominated regime. Nevertheless, as Durst et al. (2005) demonstrated, the constant in such relation still remains a function of Re , even in the apparently convection dominated regime ($Re \geq 100$) and hence numerical simulations are inevitable for all investigated ranges of parameters.

Another important observation is that irrespective of the operating condition, u_s^* in the developing region is always higher than $u_{s,fd}^*$. However, for higher Kn and C_2 , the velocity gradients at the wall are observed to be less than in the fully-developed section, which may be attributed to the presence of second term in Eq. (8) that becomes important with the increase in both Kn and C_2 . As a consequence, for such cases, the wall shear stresses in the developing region are found to be less than that in the fully-developed section, which is expected to significantly affect the variations in $K(x)$, as shall be discussed later.

3.2. Development Lengths and Correlations

The dimensionless development lengths $L_{fd}^* = L_{fd}/D_h$ for both pipe and channel flows are still characterised by the low and the high Re asymptotes, similar to that reported by Durst et al. (2005) for $Kn = 0$. The results for $Kn = 0.2$ with $C_2 = 0$ and $C_2 = 0.5$, along with that for $Kn = 0$, are presented in Fig. 4. A careful examination of the results, which will be shortly evident from the data in Table 1, shows that except for pipe flows in the high Re regime and for both pipe and channel flows in the low Re regime only with $C_2 = 0$ and high Kn , L_{fd}^* increases with the increase in both Kn and C_2 . In the high Re regime, however, irrespective of C_2 , L_{fd}^* for pipe flows first decreases with the initial increase in Kn , where both reduction in L_{fd}^* and value of Kn , up to which L_{fd}^* decreases, depend on C_2 . With the subsequent increase in Kn , L_{fd}^* increases irrespective

of C_2 , although only for the first order velocity slip condition ($C_2 = 0$), L_{fd}^* decreases once again with the further increase in Kn . Similar behaviour, however, could not be detected for channel flows, irrespective of C_2 . In the low Re regime, on the other hand, L_{fd}^* for both pipe and channel flows only with $C_2 = 0$ has been found to decrease marginally for higher values of Kn . For all other C_2 , L_{fd}^* in the diffusion dominated regime consistently increases with the increase in kn . Nevertheless, the intermediate data are not presented in Fig. 4 for brevity, since they will be shortly apparent from the proposed correlations and the asymptotic behaviours for $Re \rightarrow 0$ and $Re \rightarrow \infty$ in Table 1.

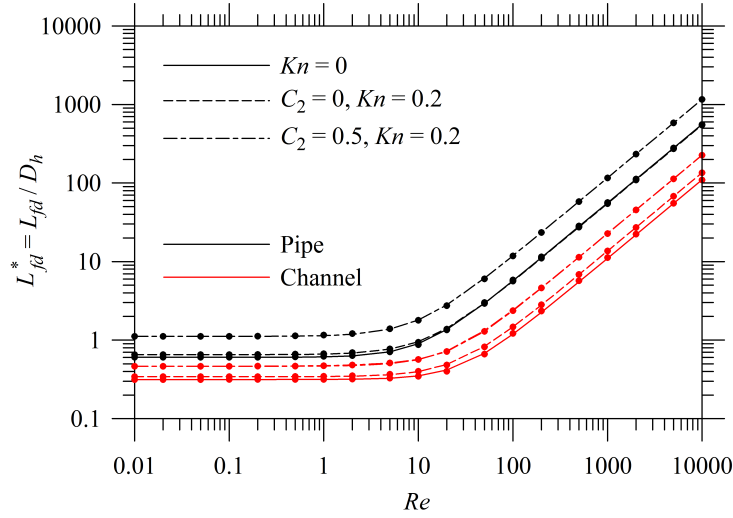


Figure 4: $L_{fd}^* = L_{fd}/D_h$ as functions of Re . The symbols represent the raw computational data and the lines are obtained according to Eq. (19).

Comparing the variations in L_{fd}^* for $Kn = 0$ and 0.2 , it may be concluded that earlier correlations, developed specifically for the continuum regime (Chen, 1973; Dombrowski et al., 1993; Durst et al., 2005), cannot be used for predicting L_{fd}^* of flows in presence of velocity slip at the wall, without causing substantial error. Nevertheless, the dependence of L_{fd}^* on Re could still be represented in its general form as:

$$L_{fd}^* = [(L_0)^q + (L_1 Re)^q]^{1/q} \quad (19)$$

where L_0 and L_1 are functions of Kn and C_2 . They could also be functions of C_1 . However, since C_1 has been kept fixed to unity for all investigated cases, its effect could not be

ascertained from the present study. Nevertheless, L_0 and L_1 have been directly obtained from the simulated data for L_{fd}^* at $Re = 10^{-2}$ and L_{fd}^*/Re at $Re = 10^4$, respectively. The results for different combinations of C_2 and Kn are presented in Table 1 for completeness, where the minimum L_1 for all C_2 and the local maximum L_1 for $C_2 = 0$ are highlighted for easy identification of the features described earlier.

As compared to the correlations proposed by Durst et al. (2005) for $Kn = 0$, certain values have been further adjusted in order to improve the predictability. The exponent q has been found to be 1.5975 and 1.6002 for pipe and channel flows, respectively, instead of 1.6 for both geometries in Eq. (2).⁷ For pipe flows, $L_0 = 0.6044$ (instead of 0.619 with 2.42 % deviation) and $L_1 = 5.5935 \times 10^{-2}$ (rather than 5.67×10^{-2} with 1.37 % deviation) have been determined with a maximum absolute error of 2.47 %, in contrast to 4.38 %, obtained from the correlation of Durst et al. (2005). Similarly, for channel flows, $L_0 = 0.3152$ (as opposed to 0.3155, with 0.1 % deviation) and $L_1 = 1.0984 \times 10^{-2}$ (in lieu of 1.105×10^{-2} with 0.6 % deviation) have been evaluated with a maximum absolute error of 3.86 %, as compared to 4.16 % achieved according to Eq. (2).

Insignificant deviations in the exponent q has been observed since the earlier correlations (Durst et al., 2005) were obtained by allowing q to vary only up to the first place of decimal, while minimising the maximum absolute relative error in L_{fd}^* using a search method. The marginal variations in L_1 may be explained by the fact that the earlier high Re asymptotes were obtained for $Re = 4 \times 10^3$, whereas the present computations have been extended up to $Re = 10^4$. On the other hand, small differences in L_{fd}^* for $Re \rightarrow 0$, given by L_0 , may be attributed to the use of non-uniform grid in the radial (or the transverse) direction that better resolves the velocity gradients close to the wall than on uniform grid, employed by Durst et al. (2005). Nevertheless, the dependence of L_0

⁷Corrected up to the first place of decimal, both exponents are, however, equal to 1.6.

and L_1 on Kn for a fixed C_2 could be expressed as:

$$L_i = \sum_{j=0}^2 l_{ij} Kn^j = l_{i0} + l_{i1}Kn + l_{i2}Kn^2 \quad \text{for } i = 1, 2 \quad (20)$$

where $l_{00} = 0.6044$ and 0.3152 , while $l_{10} = 5.5935 \times 10^{-2}$ and 1.0984×10^{-2} are constants, obtained directly from the numerical simulations with $Kn = 0$ for pipe and channel flows, respectively. Other l_{0j} and l_{1j} for $j = 1$ and 2 have been found to be best represented by the quadratic functions of C_2 . For pipe flows, they have been obtained as:

$$l_{01} = 0.7937 + 1.652 C_2 - 2.1152 C_2^2 \quad (21a)$$

$$l_{02} = -2.7519 + 2.2478 C_2 + 35.8177 C_2^2 \quad (21b)$$

$$l_{11} = 7.691 \times 10^{-4} + 0.2212 C_2 - 0.2954 C_2^2 \quad (21c)$$

$$l_{12} = -3.3061 \times 10^{-2} + 0.3009 C_2 + 4.8206 C_2^2 \quad (21d)$$

Similarly, for channel flows, these coefficients have been correlated as:

$$l_{01} = 0.4189 + 0.4671 C_2 + 1.8294 \times 10^{-2} C_2^2 \quad (22a)$$

$$l_{02} = -1.4249 + 3.1608 C_2 + 1.2335 C_2^2 \quad (22b)$$

$$l_{11} = 2.1484 \times 10^{-2} + 2.2458 \times 10^{-2} C_2 - 6.637 \times 10^{-3} C_2^2 \quad (22c)$$

$$l_{12} = -4.312 \times 10^{-2} + 0.2681 C_2 + 0.1863 C_2^2 \quad (22d)$$

The exponent q in Eq. (19) has been found to vary between 1.5975 and 1.4992 for pipe flows and 1.6002 and 1.4923 for channel flows. Similar to Durst et al. (2005), these values have been obtained by minimising the maximum absolute relative error in L_{fd}^* for different combinations of Kn and C_2 . Since the predicted L_{fd}^* is less sensitive to the variations in q and since q varies over a relatively small range, it has been correlated as:

$$q = 1.5975 - (0.4956 - 0.6511 C_2 + 0.7115 C_2^2) Kn \quad \text{for pipe} \quad (23a)$$

$$= 1.6002 - (0.5743 - 0.9495 C_2 + 0.7444 C_2^2) Kn \quad \text{for channel} \quad (23b)$$

The performance of the correlations is presented in Fig. 5 for the most stringent case with $Kn = 0.2$ for different C_2 and also for $Kn = 0$, similar to that obtained by Durst et al. (2005) in the continuum regime. It is evident from the figure that irrespective of Re , Kn

and C_2 , the present correlations perform extremely well for both geometries and produce maximum absolute errors of 2.47 % and 3.86 % for pipe and channel flows, respectively. Comparing these deviations with that obtained earlier for the continuum regime, it is obvious that the maximum errors in prediction occur for $Kn = 0$ for both pipe and channel flows and hence the exponent q may be further adjusted.

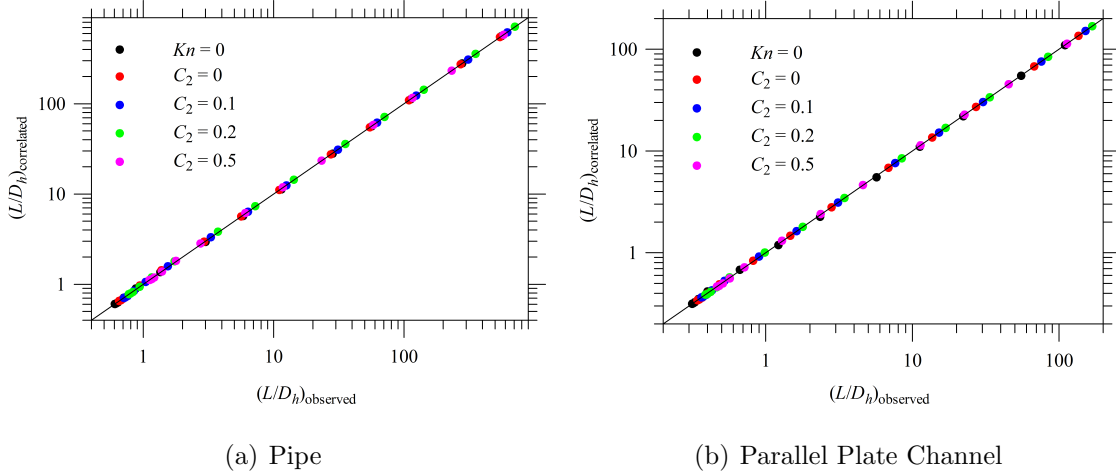


Figure 5: Performance of the correlations for L_{fd}^* . The solid lines represent 100% accuracy.

At this point, it may be mentioned that instead of evaluating q from Eq. (23), if constant values of $q = 1.5975$ and 1.6002 are used irrespective of C_2 and Kn , the resultant correlations produce maximum errors of 3.65 % (for $C_2 = 0.1$ and $Kn = 0.2$) and 3.86 % (for $Kn = 0$) for pipe and channel flows, respectively. On the other hand the use of $q = 1.6$ for both pipe and channel flows, as proposed by Durst et al. (2005) for the continuum regime, yields maximum absolute errors of 3.70 % and 3.87 % for pipe and channel flows, respectively.⁸ Therefore, if some additional error (≈ 1.23 %) is considered acceptable for pipe flows, $q = 1.6$ may be recommended for both geometries in order to correlate L_{fd}^* even in the presence of substantial velocity slip at the wall, provided L_0 and L_1 are evaluated according to Eq. (20), while calculating l_{ij} from Eqs. (21) and (22) for pipe and channel flows, respectively.

⁸The maximum absolute error for pipe flows is still less than that for channel flows.

For completeness, a comparison of the present correlation for channel flows with the first order velocity slip condition at the wall⁹ with those proposed by Barber and Emerson (2001) and Ferrás et al. (2012) is presented in Fig. 6 for $Kn = 0.2$. The figure clearly shows that although the high Re asymptote is well represented by both Eqs. (3a) and (19), the correlation of Ferrás et al. (2012) in Eq. (3b) deviates considerably from the simulated data for $Re > 200$. Nevertheless, up to $Re = 200$, all correlations perform almost equally well and hence they are hardly distinguishable from each other in Fig. 6. The maximum absolute errors for $Kn = 0.2$, however, have been obtained as 1.76 %, 3.06 % and 2.21 % for the present correlation (for $10^{-2} \leq Re \leq 10^4$), Eq. (3a) (for $10^{-2} \leq Re \leq 400$) and Eq. (3b) (for $10^{-2} \leq Re \leq 200$), respectively. For $Kn = 0$, on the other hand, these errors are found to be 3.86 %, 8.59 % and 6.98 %, respectively, for $10^{-2} \leq Re \leq 10^4$, although these variations are not shown in Fig. 6 for brevity. It may, therefore, be safely concluded that the present correlation for channel flows is not only more general¹⁰ as compared to the recommendations from earlier studies, but also it has been proved to be the most accurate over the entire ranges of investigated parameters.

For pipe flows, however, no realistic comparison could be made since the only investigation from Barber and Emerson (2001) recommended using the earlier correlations from Chen (1973) and Dombrowski et al. (1993) that were specifically developed for $Kn = 0$ in the continuum regime, even for $Kn \neq 0$. Therefore, the present correlations in Eq. (19) are recommended for evaluating L_{fd} for both pipe and channel flows.

3.3. Incremental Pressure Drop Number

The investigation on pressure drop in the entrance region of micro-channels has been carried out by analysing the variations in $K(x)$ as functions of x/D_h for different operating conditions and their asymptotic behaviour in the fully-developed section has been analysed from the variations in K_{fd} as functions of Re , Kn and C_2 . While L_{fd}^* for $Kn \neq 0$

⁹obtained by setting $C_2 = 0$

¹⁰Since it accounts for the second order velocity slip condition at the wall.

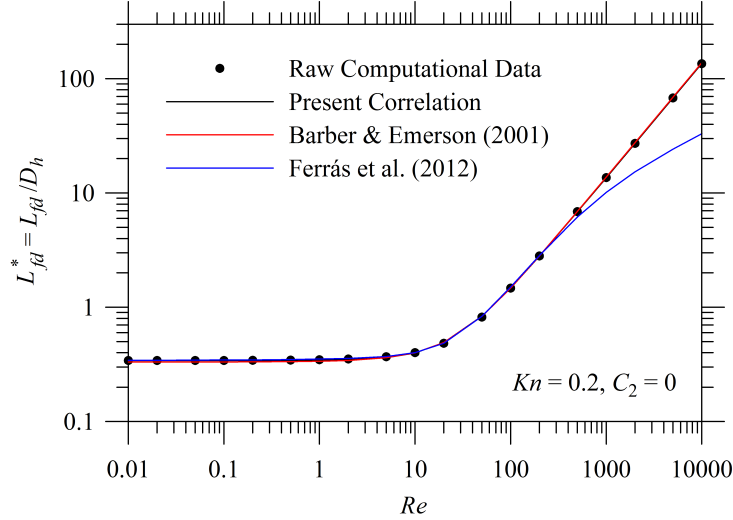


Figure 6: Comparison of different correlations for L_{fd}^* for channel flows with $Kn = 0.2$ and $C_2 = 0$.

qualitatively remains similar to that for the no-slip case with $Kn = 0$ and hence could still be functionally represented by the similar form in Eq. (19), substantial qualitative differences have been observed in the pressure drop data. In this section, the variations in $K(x)$ and K_{fd} are critically examined and the correlations for the latter, that are extremely important for the evaluation of pressure drop for $L \geq L_{fd}$, are proposed.

For pipe flows with first order velocity slip condition at the wall, i.e., with $C_2 = 0$, the variations in $K(x)$ for different Re and Kn are presented in Fig. 7, from which, it is evident that irrespective of Kn and Re , $K(x)$ always increases from 0 at $x^* = 0$ to its asymptotic value K_{fd} for the fully-developed flow as $x^* \rightarrow \infty$, or, to be precise, for $x^* \geq L_{fd}^*$. These variations are similar to that observed for $Kn = 0$ with no-slip condition at the wall, although the magnitude of K_{fd} , as well as $K(x)$ for a particular x^* , reduces considerably with the increase in Kn . The reduction in K_{fd} is due to the decrease in both $\Delta p_{m,\infty}^*$, which, as shown in Eq. (15) and Fig. 2, is independent of Re and depends only on Kn for a given C_2 , and the velocity gradient and hence the shear stress at the wall, which, other than Kn and C_2 , also depends on Re , as demonstrated in Fig. 3. These effects are more prominent as Kn increases beyond 0.01.

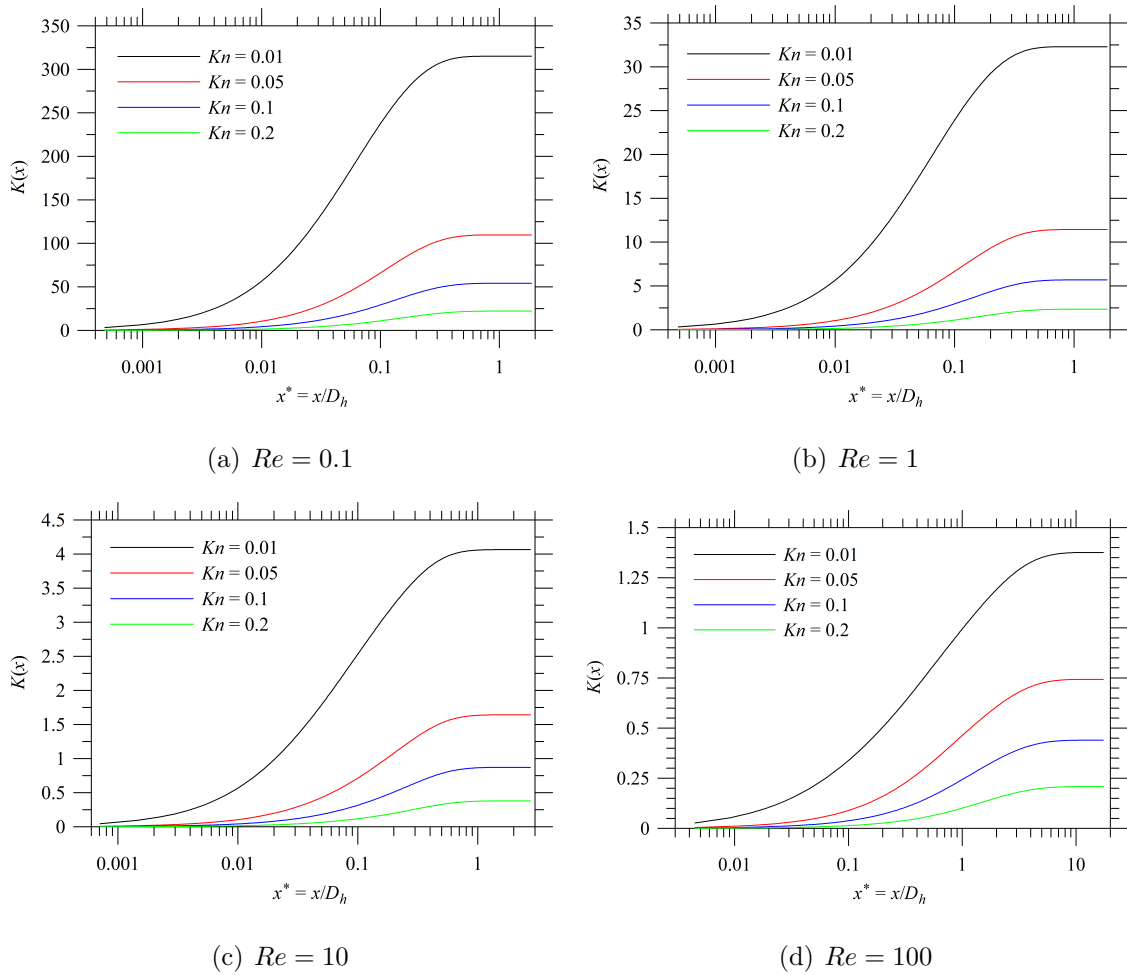


Figure 7: Effects of Kn on variations in $K(x)$ as functions of x/D_h for pipe flows with $C_2 = 0$.

Similar variations in Fig. 8 for the second order velocity slip condition at the wall with $C_2 = 0.5$, however, show some never reported interesting features. It is observed that $K(x)$ as well as K_{fd} , particularly for higher Kn , could even be negative, which, other than the already reported decrease in $\Delta p_{m,x}^*$ in Eq. (14), could be attributed to the reduction in wall shear stresses that occurs with the increase in both Kn and C_2 (see Fig. 3). It may be recognised that a positive $K(x)$, which is most often the case in the continuum regime for $Kn \leq 0.01$ and with the first order velocity slip condition ($C_2 = 0$), implies that if one calculates the true pressure drop using f_{fd} rather than $f_{app,x}$ given in Eq. (16), one would underestimate Δp , while a negative $K(x)$ would lead to an overestimation of Δp using the same method, which in certain cases, could be more acceptable than any underestimation.

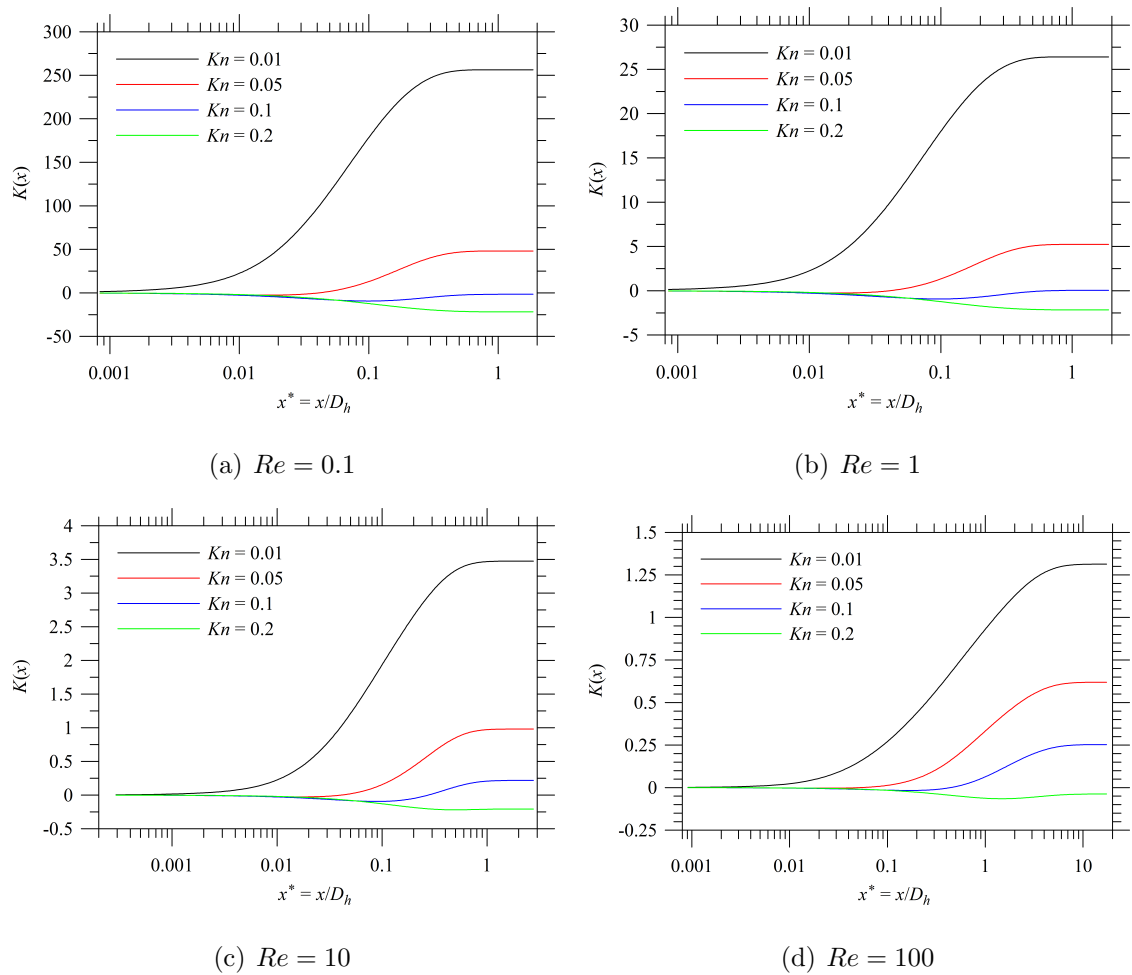


Figure 8: Effects of Kn on variations in $K(x)$ as functions of x/D_h for pipe flows with $C_2 = 0.5$.

Since negative values of $K(x)$ are observed only for higher Kn with the second order velocity slip condition at the wall, the variations in $K(x)$ with $Kn = 0.2$ for different Re and C_2 are presented in Fig. 9. The figure clearly shows that irrespective of Re , K_{fd} is always negative for $C_2 = 0.5$, whereas for lower values of C_2 (specifically for $C_2 = 0$ and 0.1 in Fig. 9), K_{fd} is always positive, although $K(x)$ for $C_2 = 0.1$ always remains negative in the entrance region. Similar variations in $K(x)$ and K_{fd} for $C_2 = 0.2$, on the other hand, show that although $K(x)$ is always negative at least in the developing region of the pipe, K_{fd} remains negative for lower Re (see cases with $Re = 0.1$ and 1 in Fig. 9), while it increases with the increase in Re and eventually becomes positive for higher Re (see results for $Re = 10$ and 100 in Fig. 9).

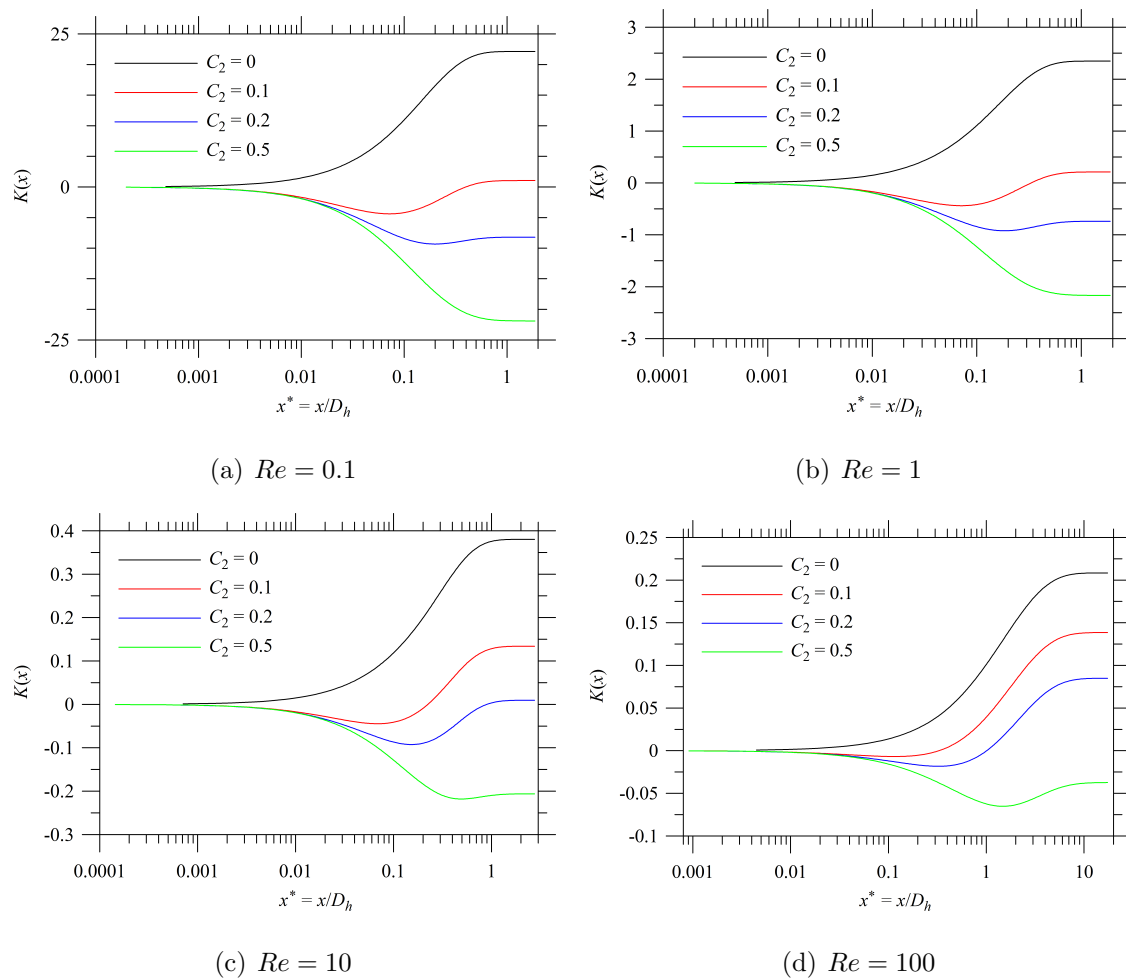


Figure 9: Effects of C_2 on variations in $K(x)$ as functions of x/D_h for pipe flows with $Kn = 0.2$.

Similar variations in $K(x)$ for $Kn = 0.01$, which lies in the border-line between the continuum and the slip flow regimes (Schaaf and Chambre, 1961), with $Re = 0.1$ and 100 are presented in Fig. 10 for different C_2 . For brevity, the intermediate results for $Re = 1$ and 10 are not presented. The comparison of results in Figs. 7 – 10 clearly shows that although $K(x)$ could be negative for higher Kn , irrespective of Re and C_2 , it always remains positive as Kn is reduced to 0.01. Most importantly, no negative $K(x)$, and hence K_{fd} , could be detected for the first order velocity slip condition at the wall, irrespective of Re and Kn .

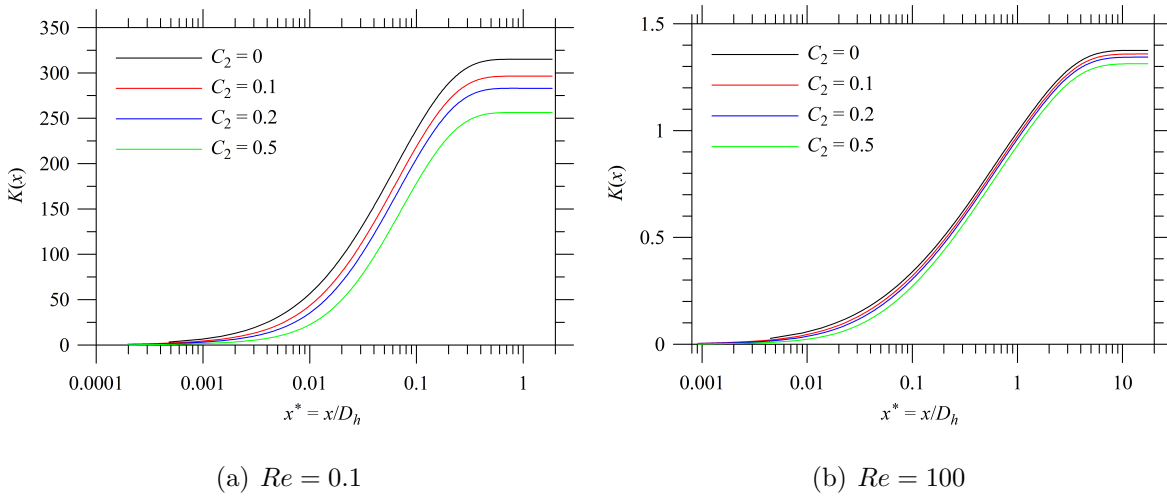


Figure 10: Effects of C_2 on variations in $K(x)$ as functions of x/D_h for pipe flows with $Kn = 0.01$.

Another apparently inconsequential general observation from Figs. 7 – 10, which has not been mentioned so far, is that for a given combination of Kn and C_2 , both $K(x)$ for a particular x^* and K_{fd} decrease substantially with the increase in Re . Such variations are, however, expected since according to Eq. (17), $K(x)$ is defined as the difference between the true and the expected fully-developed pressure drops that is normalised with respect to $\rho u_{av}^2/2$, where by definition, for a given D_h and the working fluid, u_{av} is a linearly increasing function of Re . Therefore, any reduction in $K(x)$ or K_{fd} does not necessarily imply a corresponding decrease in $\Delta p_x - \Delta p_{fd}$ and as such, Δp_x should always be calculated according to Eq. (18).

The aforementioned observations may be summarised as follows. The generalised slip

boundary condition allows a positive tangential velocity component at the wall that, other than the operating conditions, depends on the axial location. As a consequence, with the increase in both Kn and C_2 , the normal gradient of axial velocity at the wall decreases for a given combination of Re and x^* . Therefore, the corresponding wall shear stress $\tau_{w,x}$ and hence as a consequence of Eq. (11), the local friction factor f_x are reduced. Finally, certain operating conditions can produce sufficient velocity slip at the wall that, owing to the complex interaction of three terms in Eq. (17), may eventually lead to not only negative $K(x)$ in the entrance region, but also a negative K_{fd} .

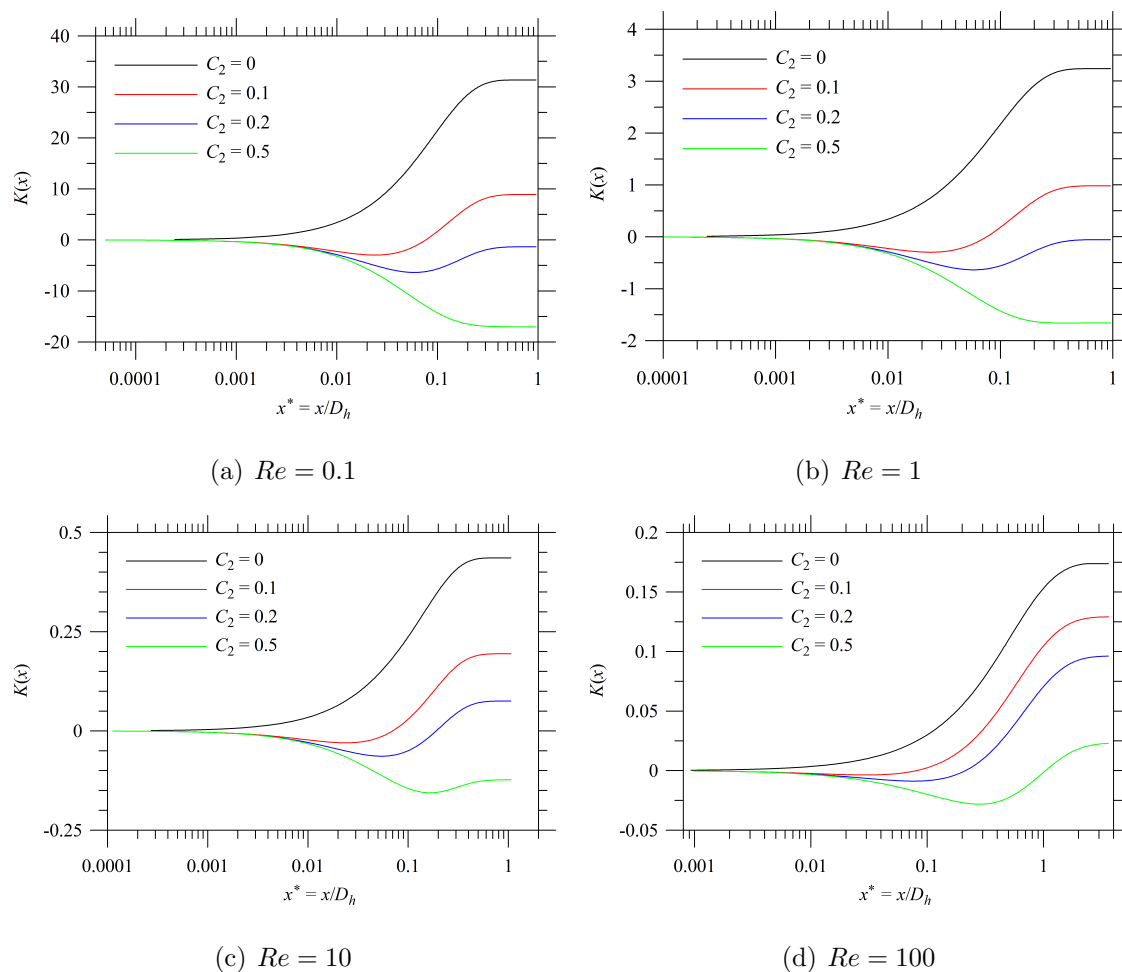


Figure 11: Effects of C_2 on variations in $K(x)$ as functions of x/D_h for channel flows with $Kn = 0.2$.

In order to demonstrate that the pressure drop characteristics for channel flows qualita-

tively remain nearly the same as that for pipe flows, the variations in $K(x)$ as functions of x^* are presented in Fig. 11 with $Kn = 0.2$ for different Re and C_2 . Comparison of results in Figs. 9 and 11 adequately substantiates the claim and for brevity, no further variations in $K(x)$ for channel flows is presented in this article. Nevertheless, it is also obvious from Figs. 7 – 11 that for both pipe and channel flows, the variations in $K(x)$ are quite complex functions of x^* and their nature strongly depends on the operating condition. Therefore, at this point, no general functional form could be proposed that would adequately describe the observed variations in $K(x)$ and hence this issue has been left beyond the scope of the present investigation.

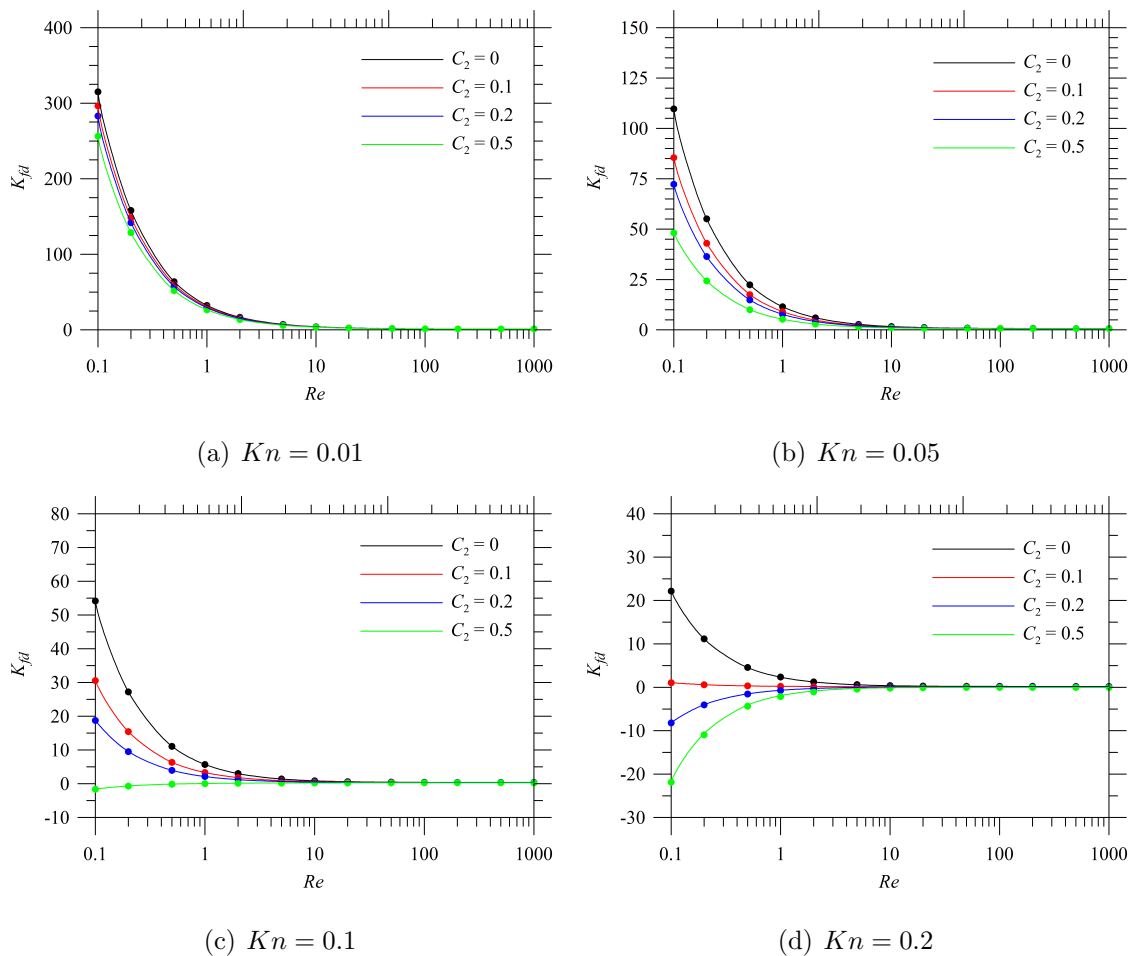


Figure 12: Effects of C_2 on variations in K_{fd} as functions of Re for Pipe flows with different Kn . The symbols represent the simulated data and the lines are obtained according to Eq. (24).

As mentioned earlier in section 2, for a duct length $L \geq L_{fd}$, the actual pressure drop Δp_L may be evaluated according to Eq. (18) by substituting $K(L) = K_{fd}$ and $x^* = L^*$. Therefore, similar to L_{fd}^* , K_{fd} is also considered as another important characteristic of the developing flow through ducts that takes into account the pressure drop in the entrance region. The variations in K_{fd} as functions of Re for different Kn and C_2 are presented in Figs. 12 and 13 for pipe and channel flows, respectively. It is evident from the figures that the magnitude of K_{fd} decreases considerably with the increase in Re , kn and C_2 , although in the high Re regime, $K_{fd} \rightarrow K_1$ and appears to be a weak function of Kn and C_2 . In addition, for lower Kn , K_{fd} is less sensitive to the change in C_2 and the sensitivity increases with the increase in Kn . Since these observations may be explained in view of the foregoing discussions, they are not repeated here for brevity.

Figures 12 and 13 also clearly show that for lower Kn , irrespective of Re and C_2 , K_{fd} is always positive, whereas for $Kn = 0.2$, depending upon C_2 and Re , K_{fd} could assume either positive or negative values. However, as mentioned earlier, for the first order velocity slip condition at the wall ($C_2 = 0$), or, even for lower C_2 , K_{fd} remains always positive for both pipe and channel flows, irrespective of Re and Kn .

Nevertheless, irrespective of Kn and C_2 , the variations in K_{fd} as functions of Re are still described by two asymptotes, where the low and the high Re asymptotes are given by K_0/Re and K_1 , respectively. Similar to L_0 and L_1 , K_0 and K_1 have been obtained directly from the simulated data for $K_{fd}Re$ at $Re = 10^{-2}$ and K_{fd} at $Re = 10^4$, respectively. The obtained data for different C_2 and Kn are presented in Table 2, from which it is evident that K_0 could assume either positive or negative values for both pipe and channel flows. On the other hand, K_1 for pipe flows is marginally negative only for higher C_2 and Kn , while it remains always positive for channel flows for the investigated ranges of Kn and C_2 . As a result, K_{fd} in Figs. 12 and 13 could not be consistently presented using the logarithmic scale and in order to highlight that K_{fd} assumes considerably smaller but non-zero values as $Re \rightarrow \infty$ on a linear scale, the variations of K_{fd} in these figures are presented only for the range $1 \leq Re \leq 10^3$.

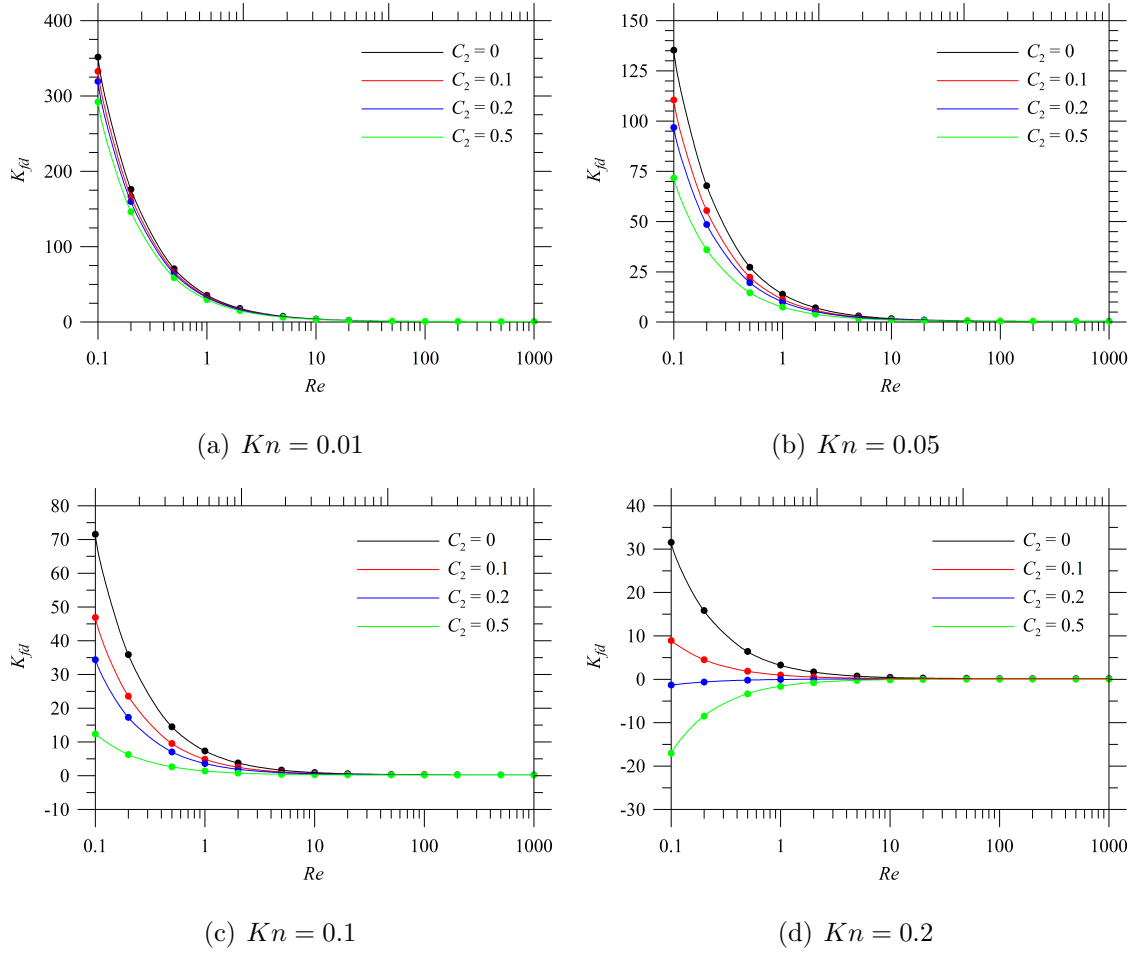


Figure 13: Effects of C_2 on variations in K_{fd} as functions of Re for Channel flows with different Kn . The symbols represent the simulated data and the lines are obtained according to Eq. (24).

Depending upon Kn and C_2 , since K_0 and K_1 assume both positive and negative values, K_{fd} could not be represented by the form similar to that for L_{fd}^* in Eq. (19). Therefore, an alternative relation, that respects both low and high Re asymptotes, has been adopted in order to correlate K_{fd} :

$$K_{fd} = \frac{K_0/Re}{1 + K_2 Re} + K_1 \quad (24)$$

where K_2 is a function of Kn and C_2 . At this point, however, it is important to note that as $x \rightarrow 0$, the wall shear stress $\tau_{w,x} \rightarrow \infty$ and it has been found to be proportional to x^{-m} . Therefore, f_x in this region is proportional to $(x^*)^{-m}$, according to the definitions of dimensionless variables. Similar consequence, although only in the convection dominated regime, could also be derived from the conventional boundary layer theory. Extensive numerical simulations show that for $Kn = 0$, m varies from 1 for $Re \rightarrow 0$, where the convective effects are insignificant, to 1/2 as $Re \rightarrow \infty$, where the axial diffusion is negligible. Therefore, for $Kn = 0$, the first term on the right hand side of Eq. (14) $\Delta p_{f,x}^* \rightarrow \infty$ as $Re \rightarrow 0$ and hence no grid-independent solution either for $K(x)$ or K_{fd} could be obtained in this limit, although L_{fd}^* has been found to attain a grid-independent value (Durst et al., 2005). Further critical appreciation of this issue, arising out of the singularity in boundary conditions at the inlet, however, has been left beyond the scope of the present article.

Nevertheless, with the increase in Kn , substantial velocity slip occurs at the wall for a given C_2 that not only reduces the wall shear stress and hence f_x close to the inlet, but also it modifies the exponent m to a great extent, from unity to reasonable fractional values, such that grid independent solutions for $K(x)$ and hence K_{fd} could be obtained even in the limit as $Re \rightarrow 0$. Therefore, correlations for K_{fd} have been obtained only for $10^{-3} \leq Kn \leq 0.2$, while accommodating the complete range of investigated Re .

In order to develop these correlations, however, K_0 and K_1 in Table 2 have been directly used, since owing to their large variations with kn and changing dependence on both Kn and C_2 , no reliable correlation for them could be derived. Subsequently, K_2 has been determined for each combination of Kn and C_2 , either by minimising the maximum

absolute relative error in K_{fd} when $|K_{fd}| \gg 0$ for the entire range of Re , or using the least square method (i.e., by maximising the coefficient of determination R^2), when $K_{fd} \approx 0$ is expected for certain Re . The latter condition could be easily identified by checking i) if $|K_1| \leq \epsilon$, where ϵ has been taken as 0.05, or ii) if the product of K_0 and K_1 is negative. Finally, for a given C_2 , K_2 as a function of Kn has been expressed as:

$$K_2 = \sum_{j=0}^2 k_{2j} Kn^j = k_{20} + k_{21} Kn + k_{22} Kn^2 \quad (25)$$

where k_{2j} are functions of C_2 . For pipe flows, they have been correlated as:

$$k_{20} = 1.778 \times 10^{-4} - 3.5265 \times 10^{-4} C_2 + 2.7782 \times 10^{-4} C_2^2 \quad (26a)$$

$$k_{21} = 1.4482 \times 10^{-1} + 1.9054 \times 10^{-1} C_2 - 1.4346 \times 10^{-1} C_2^2 \quad (26b)$$

$$k_{22} = 2.9901 C_2 + 6.2006 C_2^2 \quad (26c)$$

Similarly for channel flows, k_{2j} could be expressed as:

$$k_{00} = 1.3194 \times 10^{-4} - 1.767 \times 10^{-4} C_2 + 1.0306 \times 10^{-4} C_2^2 \quad (27a)$$

$$k_{01} = 5.3809 \times 10^{-2} + 6.1618 \times 10^{-2} C_2 - 2.412 \times 10^{-2} C_2^2 \quad (27b)$$

$$k_{02} = 1.6632 \times 10^{-1} + 1.4324 C_2 + 1.0509 C_2^2 \quad (27c)$$

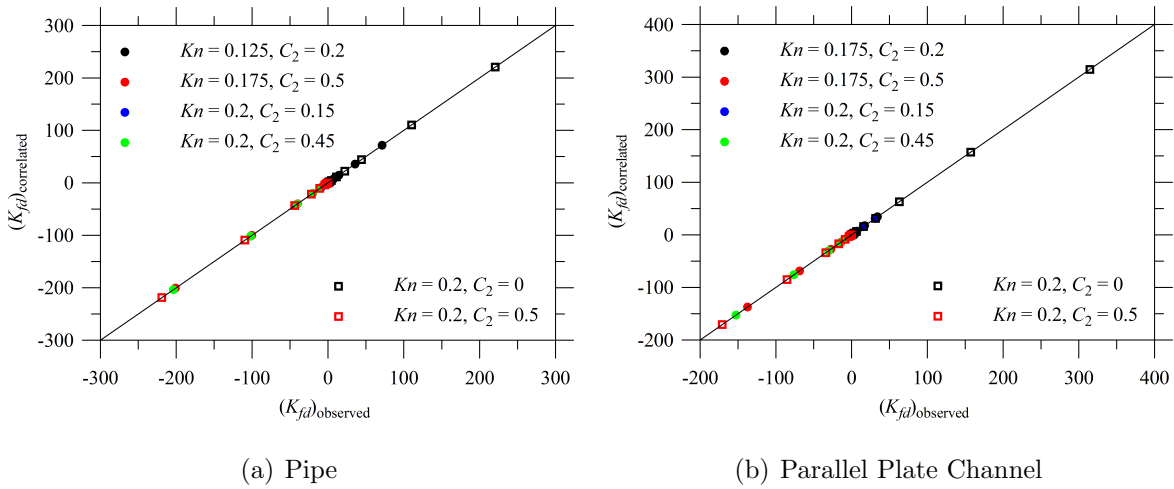


Figure 14: Performance of correlations for K_{fd} . The solid lines represent 100 % accuracy.

Since the tabulated values of K_0 and K_1 have been used in order to evaluate K_2 , the correlations for K_{fd} in Eq. (24) are expected to perform extremely well for all simulated cases. Therefore, in order to demonstrate that these correlations are still accurate for the intermediate values of Kn and C_2 , where K_0 and K_1 are required to be interpolated, four additional cases for both geometries have been carefully chosen between two tabulated results, where either K_0 or K_1 changes its sign. Comparison between the observed and the correlated values of K_{fd} for these additional cases are presented in Fig. 14. In addition, the results for two tabulated cases with $C_2 = 0$ and $C_2 = 0.5$ for $Kn = 0.2$ are also shown in the same figure in order to demonstrate that the proposed correlations indeed perform extremely well for the already reported cases, where K_0 and K_1 could be directly obtained from Table 2 without any interpolation. While quantifying the performance of the correlations, however, it must be noted that since $K_{fd} \approx 0$ has been recorded for some of the cases, the maximum absolute relative error cannot be consistently considered an appropriate measure of deviation and hence the coefficient of determination R^2 has been reported in order to demonstrate the accuracy of the correlations.

At this point, a few comments regarding the interpolation of K_0 and K_1 for intermediate Kn and C_2 are essential. It has been observed that the linearly interpolated K_0 and K_1 do not produce satisfactory agreement, owing to the non-linear nature of their variations as functions of both Kn and C_2 . The minimum values of coefficient of determination have been obtained as $R_{\min}^2 \approx 0.9$ for both pipe and channel flows,¹¹ when linear interpolation is used while considering Kn and C_2 as independent variables. In order to improve the prediction, $Kn^{1/4}$ and $C_2^{1/2}$ have been subsequently considered as independent variables for interpolation. Even then, the use of linear interpolation has resulted in $R_{\min}^2 \approx 0.96$ for both geometries, although these data are not shown in Fig. 14 for brevity. Finally,

¹¹Among four additional cases, R_{\min}^2 has been observed for $C_2 = 0.2$ with $Kn = 0.125$ and $Kn = 0.175$ for pipe and channel flows, respectively.

cubic functions¹² of $Kn^{1/4}$ and quadratic functions¹³ of $C_2^{1/2}$ have been employed for interpolating K_0 and K_1 , that, rounded up to the fourth place of decimal, produce $R^2 = 1$ for all additional cases involving both geometries.

From the foregoing discussions, it is obvious that for a duct length $L < L_{fd}$, evaluation of the actual pressure drop Δp_L from Eq. (18) requires accurate information about $K(L)$ in the developing region. However, since no correlation for $K(x)$ could be derived from the present investigation owing to its complex dependence on the operating conditions, few comments on the estimation of Δp_L for $L < L_{fd}$ would be useful. While selecting the pumping device and determining its power requirement for a particular micro-channel application, an overestimation is often considered more acceptable than any underestimation and hence in order to be on the safer side, Δp_L could be estimated as:

$$\Delta p_L = \frac{1}{2} \rho u_{av}^2 (K_{fd} + 4f_{fd}L^*) \quad \text{for } K_{fd} > 0, \text{ set } K(L) = K_{fd} \quad (28a)$$

$$= 2\rho u_{av}^2 f_{fd}L^* \quad \text{for } K_{fd} \leq 0, \text{ set } K(L) = 0 \quad (28b)$$

It must be emphasised that Δp_L , calculated from Eq. (28) for $L < L_{fd}$, should never be used for optimisation since the estimated value would always be greater than the true pressure drop and may be grossly erroneous. For $L \geq L_{fd}$, however, the correlation for K_{fd} in Eq. (24) may be used for accurately evaluating Δp_L .

4. Summary, Conclusions and Final Remarks

In the present investigation, developing laminar flows through micro-capillaries and micro-channels have been numerically analysed by solving the conventional NS equations (5) – (7) along with the second-order velocity slip condition at the wall in Eq. (8). For both

¹²In order to fit cubic functions, if possible, two points on either sides of the desired Kn have been selected (e.g., for $Kn = 0.125$ for pipe flow). Otherwise, depending upon the availability of data, three points on one side and one point on the other side of the desired Kn have been chosen (e.g., for $Kn = 0.175$ for both geometries).

¹³Quadratic functions have been fitted preferably by selecting two points on the higher side and one point on the lower side of the desired C_2 (e.g., for $C_2 = 0.15$). In the absence of such data, one point on the higher side and two points on the lower side have been chosen (e.g., for $C_2 = 0.45$).

pipe and channel flows, thorough investigations have been conducted for $10^{-2} \leq Re \leq 10^4$ and $10^{-4} \leq Kn \leq 0.2$, while specifying $C_1 = 1$ and varying C_2 from 0 to 0.5. The results for the first order velocity slip condition, similar to that presented by Barber and Emerson (2001) and Ferrás et al. (2012) for parallel plate channels, have been obtained by setting $C_2 = 0$, whereas that of Durst et al. (2005) in the continuum regime have been generated with $Kn = 0$.

Before carrying out the extensive parametric study, the maximum length x_{\max}^* of the computational domain has been first ascertained. The development of the axial velocity profile shows that analytical solutions for the fully-developed flow have always been obtained at the exit of the duct, irrespective of the operating condition. Since the obtained numerical solutions are also grid independent, this observation confirms the authenticity of the predicted results. The converged solutions for each combination of Re , Kn and C_2 have been further post-processed in order to evaluate the local friction factor f_x , the dimensionless development length L_{fd}^* , the local and the fully-developed incremental pressure drop number $K(x)$ and K_{fd} , respectively. The obtained data have been carefully analysed and correlations for L_{fd}^* and K_{fd} have been proposed for both geometries. The major conclusions from the present investigation may be summarised as follows:

1. The development of the axial velocity profile shows that although irrespective of Re , Kn and C_2 , u_s^* for any $x^* \leq L_{fd}^*$ is always higher than $u_{s,fd}^*$, the velocity gradients at the wall and hence $\tau_{w,x}$ could be considerably less than that in the fully-developed section, particularly for higher Kn and C_2 . These effects are more prominent for lower Re and significantly affect the variations in $K(x)$ and hence K_{fd} . The velocity overshoots, on the other hand, are observed to be more pronounced for higher Re with lower velocity slip at the wall and are considerably reduced with the decrease in Re as well as the increase in both Kn and C_2 .
2. The development length L_{fd}^* increases with the increase in both Kn and C_2 , except for pipe flows in the high Re regime and for both geometries in the low Re regime, but only with $C_2 = 0$. For the first exception, L_{fd}^* initially decreases and subse-

quently increases with the increase in Kn , except for $C_2 = 0$, for which, although the variation is marginal, it decreases once again. For the second exception, on the other hand, L_{fd}^* decreases marginally for higher Kn , which could be detected for $Kn = 0.2$ for both geometries.

3. Similar to the continuum regime, L_{fd}^* in the presence of second order velocity slip at the wall is also characterised by the low and the high Re asymptotes and hence it has been correlated according to Eq. (19), where the expressions for L_0 , L_1 and q are provided in Eqs. (20) – (23). The proposed correlations for L_{fd}^* produce 2.47 % and 3.86 % errors for pipe and channel flows, respectively. On the other hand, with a constant $q = 1.6$, as proposed by Durst et al. (2005), these errors are obtained as 3.70 % and 3.87 %, respectively. Even for flows through parallel plate micro-channels with the first order velocity slip condition at the wall, the present correlation has been found to be more accurate than those proposed by Barber and Emerson (2001) and Ferrás et al. (2012) for the entire range of Reynolds number.
4. Pressure drop characteristics in the entrance region as well as in the fully-developed section of micro-channels have been thoroughly analysed. It has been observed that depending upon the operating condition, particularly for higher Kn and C_2 , both $K(x)$ and K_{fd} could assume negative values. This important as well as interesting feature, which is more prominent in the low Re regime, has never been reported in the literature. These results imply that in the presence of substantial velocity slip at the wall, the pressure gradient in the developing section could be even less than that in the fully-developed region.
5. No reliable correlation for $K(x)$ could be proposed from the present investigation since for both geometries, $K(x)$ is a quite complicated function of the axial location and the functional form depends strongly on the operating condition. Although the calculation of true pressure drop for a duct of length $L < L_{fd}$ requires precise knowledge about $K(x)$, a method has been proposed in order to obtain a conservative estimate of the pressure drop that, other than the fully-developed friction factor f_{fd} , also depends on K_{fd} for $K_{fd} > 0$.
6. The magnitude of K_{fd} decreases consistently with the increase in Re , Kn and C_2 ,

although it is a weak function of Kn and C_2 in the high Re regime where $K_{fd} \rightarrow K_1$. Irrespective of C_2 , it has been found to be a strong function of Kn , whereas it appears to be weak function of C_2 for lower Kn and its sensitivity to the change in C_2 increases with the increase in Kn .

7. Similar to L_{fd}^* , the variations in K_{fd} as functions of Re are also represented by the low and the high Re asymptotes, K_0/Re and K_1 , respectively for any combination of Kn and C_2 . However, since these asymptotic values vary over a large range and their functional dependence on both Kn and C_2 changes considerably over the investigated ranges, no reliable correlation for either K_0 or K_1 could be proposed. Moreover, since K_0 for both geometries and K_1 for pipe flows assume both positive and negative values, K_{fd} could not be expressed by the form similar to that for L_{fd}^* and hence an alternative expression in Eq. (24) has been adopted that satisfies both low and high Re limits. Using the tabulated values of K_0 and K_1 , K_2 has been determined for each C_2 , while allowing Kn to vary from 10^{-3} to 0.2, from which, correlations for K_2 has been proposed that are presented in Eqs. (25) – (27).
8. Four additional cases for both geometries have been specifically simulated for intermediate values of Kn and C_2 , where K_0 and K_1 are required to be carefully interpolated using cubic functions of $Kn^{1/4}$ and quadratic functions of $C_2^{1/2}$. The performance of the proposed correlations show excellent agreement with the simulated data for all additional cases, with $R^2 = 1$ for both geometries.

As a final remark, it may be mentioned that in the present investigation, although Re , Kn and C_2 have been varied over wide ranges, C_1 has been kept fixed to unity. Previous investigations and the present analysis based on the dimensionless parameters clearly show that the effects of Kn and C_1 could not be separated if the first order velocity slip condition at the duct surface is applied. Therefore, in the future, C_1 in the second order velocity slip boundary condition at the wall should be varied over a realistic range in order to quantify its effects on both development length and pressure drop in the entrance region for pipe and channel flows.

References

- C. K. Aidun and J. R. Clausen. Lattice-Boltzmann method for complex flows. *Annual Review of Fluid Mechanics*, 42:439–472, 2010.
- S. Ansumali, I. V. Karlin, S. Arcidiacono, A. Abbas, and N. Prasianakis. Hydrodynamics beyond navierstokes: exact solution to the lattice Boltzmann hierarchy. *Physical Review Letters*, 98:124502, 2007.
- E. B. Arkilic, M. A. Schmidt, and K. S. Breuer. Gaseous slip flow in microchannels. *Journal of Microelectromechanical Systems*, 6:167–174, 1997.
- R. W. Barber and D. R. Emerson. A numerical investigation of low reynolds number gaseous slip flow at the entrance of circular and parallel plate micro-channels. In *Proceedings of ECCOMAS Computational Fluid Dynamics Conference*, 2001.
- R. W. Barber and D. R. Emerson. Challenges in modeling gas-phase flow in microchannels: from slip to transition. *Heat Transfer Engineering*, 27:3–12, 2006.
- A. Beskok and G. E. Karniadakis. Rarefaction and compressibility effects in gas microflows. *ASME J. Fluids Eng.*, 118:448–456, 1996.
- A. Beskok and G. E. Karniadakis. A model for flows in channels, pipes, and ducts at micro and nano scales. *Microscale Thermophysical Engineering*, 3:43–77, 1999.
- G. A. Bird. *Molecular gas dynamics and the direct simulation of gas flows*. Clarendon Press, Oxford, 1994.
- R. B. Bird, W. E. Stewart, and E. N. Lightfoot. *Transport Phenomena*. John Wiley & Sons, New York, 2002.
- B. Y. Cao, J. Sun, M. Chen, and Z. Y. Guo. Molecular momentum transport at fluid-solid interfaces in mems/nems: a review. *International Journal of Molecular Sciences*, 10:4638–4706, 2009.
- C. Cercignani. *Theory and application of the Boltzmann equation*. Scottish Academic Press, Edinburgh, 1975.

- C. Cercignani. *The Boltzmann equation and its applications*. Springer-Verlag, New York, 1988.
- C. Cercignani. *Mathematical methods in kinetic theory*. Plenum, New York, 1990.
- C. Cercignani. *Rarefied gas dynamics*. Cambridge University Press, Cambridge, 2000.
- S. Chakraborty and F. Durst. Derivations of extended navier-stokes equations from up-scaled molecular transport considerations for compressible ideal gas flows: Towards extended constitutive forms. *Phys. Fluids*, 19:088104, 2007.
- D. Chen and D. B. Bogy. Comparisons of slip-corrected reynolds lubrication equations for the air bearing film in the head-disk interface of hard disk drives. *Tribology Letters*, 37:191–201, 2010.
- R. Y. Chen. Flow in the entrance region at low reynolds numbers. *ASME J. Fluids Eng.*, 95:153–158, 1973.
- S. Colin. Rarefaction and compressibility effects on steady and transient gas flows in microchannels. *Microfluidics and Nanofluidics*, 1:268–279, 2005.
- S. Colin. Gas microflows in the slip flow regime: a critical review on convective heat transfer. *ASME Journal of Heat Transfer*, 134:020908, 2012.
- R. Cornubert, D. d’Humieres, and D. Levermore. A knudsen layer theory for lattice gases. *Physica D*, 47:241–259, 1991.
- N. Dombrowski, E. A. Foumeny, S. Ookawara, and A. Riza. The influence of reynolds number on the entry length and pressure drop for laminar pipe flow. *The Canadian Journal of Chemical Engineering*, 71:472–476, 1993.
- N. Dongari, A. Agrawal, and A. Agrawal. Analytical solution of gaseous slip flow in long microchannels. *Int. J. Heat Mass Transfer*, 50:3411–3421, 2007.
- N. Dongari, R. Sambasivam, and F. Durst. Extended navierstokes equations and treatments of micro-channel gas flows. *Journal of Fluid Science and Technology*, 4:454–467, 2009.

- N. Dongari, F. Durst, and S. Chakraborty. Predicting microscale gas flows and rarefaction effects through extended navierstokesfourier equations from phoretic transport considerations. *Microfluidics and Nanofluidics*, 9:831–846, 2010.
- N. Dongari, Y. H. Zhang, and J. M. Reese. Molecular free path distribution in rarefied gases. *Journal of Physics D, Applied Physics*, 44:125502, 2011a.
- N. Dongari, Y. H. Zhang, and J. M. Reese. Modeling of knudsen layer effects in micro/nanoscale gas flows. *ASME J. Fluids Eng.*, 133:071101, 2011b.
- F. Durst, B. Ünsal, S. Ray, and O. Saleh. The development lengths of laminar pipe and channel flows. *ASME J. Fluids Eng.*, 127:1154–1160, 2005.
- L. Ferrás, A. Alfonso, M. Alves, J. Nóbrega, and F. Pinho. Development length in planar channel flows of newtonian fluids under the influence of wall slip. *ASME J. Fluids Eng.*, 134:104503–1–104503–5, 2012.
- J. H. Ferziger and M. Perić. *Computational Methods for Fluid Dynamics*. Springer, Berlin, 1999.
- R. W. Fox, A. T. McDonald, and P. J. Pritchard. *Introduction to Fluid Mechanics*. John Wiley & Sons, New York, 2010.
- M. Gad-el-Hak. The fluid mechanics of microdevices - the freeman scholar lecture. *JFE*, 121:5–33, 1999.
- M. Gad-el-Hak. Flow physics in mems. *Mécanique & Industries*, 2:313–341, 2001.
- M. Gad-el-Hak. Gas and liquid transport at the microscale. *Heat Transfer Engineering*, 27:13–29, 2006.
- N. G. Hadjiconstantinou. Analysis of discretization in the direct simulation monte carlo. *Phys. Fluids*, 12:2634–2638, 2000.
- N. G. Hadjiconstantinou. The limits of navierstokes theory and kinetic extensions for describing small-scale gaseous hydrodynamics. *Phys. Fluids*, 18:111301, 2006.

- C. M. Ho and Y. C. Tai. Micro-electro-mechanical-systems (mems) and fluid flows. *Annual Review of Fluid Mechanics*, 30:579–612, 1998.
- S. Jin and M. Slemrod. Regularization of the burnett equations via relaxation. *Journal of Statistical Physics*, 103:1009–1033, 2001.
- S. G. Kandlikar, S. Colin, Y. P. S. Garimella, R. F. Pease, J. J. Brandner, and D. B. Tuckerman. Heat transfer in microchannels - 2012 status and research needs. *ASME Journal of Heat Transfer*, 135:091001, 2013.
- G. E. Karniadakis and A. Beskok. *Micro flows: fundamentals and simulation*. Springer-Verlag, New York, 2002.
- G. E. Karniadakis, A. Beskok, and N. Aluru. *Microflows and Nanoflows: Fundamentals and Simulation*. Springer-Verlag, New York, 2005.
- P. K. Khosla and S. G. Rubin. A diagonally dominant second order accurate implicit scheme. *Comput. Fluids*, 2:207–209, 1974.
- M. Knudsen. Die gesetze der molekularströmung und der inneren reibungsströmung der gase durch röhren. *Annalen der Physik*, 333(1):75–130, 1909.
- B. Li and D. Y. Kwok. Discrete Boltzmann equation for microfluidics. *Physical Review Letters*, 90:124502, 2003.
- C. R. Lilley and J. E. Sader. Velocity profile in the knudsen layer according to the Boltzmann equation. *Proceedings of Royal Society A*, 464:2015–2035, 2008.
- D. A. . Lockerby and J. M. Reese. On the modelling of isothermal gas flows at the microscale. *J. Fluid Mechanics*, 604:235–261, 2008.
- D. A. Lockerby, J. M. Reese, D. R. Emerson, and R. W. Barber. Velocity boundary condition at solid walls in rarefied gas calculations. *Physical Review E*, 70:017303, 2004.
- S. K. Loyalka. Approximate method in kinetic theory. *Phys. Fluids*, 14:2291–2294, 1971.

- L. S. Pan, G. R. Liu, and K. Y. Lam. Determination of slip coefficient for rarefied gas flows using direct simulation monte carlo. *Journal of Micromechanics and Microengineering*, 9:89–96, 1999.
- S. V. Patankar. *Numerical Heat Transfer and Fluid Flow*. Hemisphere, Washington, DC, 1980.
- S. V. Patankar and D. B. Spalding. A calculation procedure for heat, mass and momentum transfer in three-dimensional parabolic flows. *Int. J. Heat Mass Transfer*, 15(10):1787–1806, 1972.
- C. Rhie and W. Chow. Numerical study of the turbulent flow past an airfoil with trailing edge separation. *AIAA J.*, 21(11):1525–1532, 1983.
- E. Roohi and M. Darbandi. Extending the navierstokes solutions to transition regime in two-dimensional micro- and nanochannel flows using information preservation scheme. *Phys. Fluids*, 21:082001, 2009.
- R. Sambasivam. *Extended Navier-Stokes Equations: Derivations and Applications to Fluid Flow Problems*. PhD thesis, Friedrich Alexander Universität, Erlangen-Nürnberg, Germany, 2013.
- M. Sbragaglia and Succi. Analytical calculation of slip flow in lattice Boltzmann models with kinetic boundary conditions. *Phys. Fluids*, 17:093602, 2005.
- S. A. Schaaf and P. L. Chambre. *Rarefied Gas Dynamics*. Princeton University Press, Princeton, 1961.
- R. K. Shah and A. L. London. *Advances in Heat Transfer, Supplement I: Laminar Flow Forced Convection in Ducts*. Academic Press, New York, San Francisco, London, 1978.
- X. Shan, X. Yuan, and H. Chen. Kinetic theory representation of hydrodynamics: a way beyond the navierstokes equation. *J. Fluid Mechanics*, 550:413–441, 2006.

- F. Sharipov. Application of the cercignani-lampis scattering kernel to calculations of rarefied gas flows. ii. slip and jump coefficients. *European Journal of Mechanics B/Fluid*, 22:133–143, 2003.
- F. Sharipov and V. Seleznev. Data on internal rarefied gas flows. *J Phys Chem Ref Data*, 27:657–706, 1998.
- C. E. Siewert and F. Sharipov. Model equations in rarefied gas dynamics: Viscous-slip and thermal-slip coefficients. *Phys. Fluids*, 14:4123–4129, 2002.
- H. L. Stone. Iterative solution of implicit approximations of multidimensional partial differential equations. *SIAM. J. Num. Anal.*, 5:530–541, 1968.
- H. Struchtrup and M. Torrilhon. Regularization of grids 13 moment equations: derivation and linear analysis. *Phys. Fluids*, 15:2668–2680, 2003.
- H. Struchtrup and M. Torrilhon. Higher-order effects in rarefied channel flows. *Physical Review E*, 78:046301, 2008.
- G. H. Tang, Y. L. He, and W. Q. Tao. Comparison of gas slip models with solutions of linearized Boltzmann equation and direct simulation of monte carlo method. *International Journal of Modern Physics C*, 18:203–216, 2007a.
- G. H. Tang, L. Zhuo, Y. L. He, and W. Q. Tao. Experimental study of compressibility, roughness and rarefaction influences on microchannel flow. *Int. J. Heat Mass Transfer*, 50:2282–2295, 2007b.
- G. H. Tang, Y. H. Zhang, and D. R. Emerson. Lattice Boltzmann models for nonequilibrium gas flows. *Physical Review E*, 77:046701, 2008.
- H. C. Weng and C. K. Chen. A challenge in navierstokes-based continuum modeling: Maxwell-burnett slip law. *Phys. Fluids*, 20:106101, 2008.
- F. M. White. *Fluid Mechanics*. McGraw-Hill, New York, 2003.
- L. Wu and D. B. Bogy. A generalized compressible reynolds lubrication equation with bounded contact pressure. *Phys. Fluids*, 13:2237–2244, 2001.

- H. W. Zhang, Z. Q. Zhang, Y. G. Zheng, and H. F. Ye. Molecular dynamics-based prediction of boundary slip of fluids in nanochannels. *Microfluidics and Nanofluidics*, 12:107–115, 2012a.
- J. Zhang. Lattice Boltzmann method for microfluidics: models and applications. *Microfluidics and Nanofluidics*, 10:1–28, 2011.
- R. Zhang, X. Shan, and H. Chen. Efficient kinetic method for fluid simulation beyond the navierstokes equation. *Physical Review E*, 74:046703, 2006a.
- W. Zhang, G. Meng, and X. Wei. A review on slip models for gas microflows. *Microfluidics and Nanofluidics*, 13:845–882, 2012b.
- Y. H. Zhang, X. J. Gu, R. W. Barber, and D. R. Emerson. Capturing knudsen layer phenomena using a lattice Boltzmann model. *Physical Review E*, 74:046704, 2006b.
- Y. Zheng, J. M. Reese, T. J. Scanlon, and D. A. Lockerby. Scaled navier-stokes-fourier equations for gas flow and heat transfer phenomena in micro- and nanosystems. In *Proceedings of ASME ICNMM2006*, Limerick, Ireland 96066, June 19–21 2006.

Table 1: L_0 and L_1 for different C_2 and Kn .

	Kn	$C_2 = 0$		$C_2 = 0.1$		$C_2 = 0.2$		$C_2 = 0.3$		$C_2 = 0.4$		$C_2 = 0.5$	
		L_0	$L_1/10^{-2}$	L_0	$L_1/10^{-2}$	L_0	$L_1/10^{-2}$	L_0	$L_1/10^{-2}$	L_0	$L_1/10^{-2}$	L_0	$L_1/10^{-2}$
Pipe	0	0.6044	5.5935	0.6044	5.5935	0.6044	5.5935	0.6044	5.5935	0.6044	5.5935	0.6044	5.5935
	0.0001	0.6045	5.5931	0.6045	5.5931	0.6045	5.5931	0.6045	5.5931	0.6045	5.5931	0.6045	5.5931
	0.001	0.6054	5.5882	0.6054	5.5884	0.6054	5.5884	0.6054	5.5882	0.6054	5.5882	0.6054	5.5882
	0.01	0.6136	5.5757	0.6138	5.5795	0.6141	5.5840	0.6144	5.5888	0.6146	5.5934	0.6149	5.5981
	0.02	0.6220	5.5795	0.6232	5.5975	0.6244	5.6159	0.6256	5.6344	0.6268	5.6543	0.6281	5.6743
	0.05	0.6399	5.5918	0.6471	5.6894	0.6544	5.7903	0.6623	5.8943	0.6703	6.0014	0.6786	6.1116
	0.1	0.6531	5.5768	0.6756	5.8708	0.6999	6.1890	0.7263	6.5322	0.7550	6.9053	0.7866	7.3167
	0.15	0.6554	5.5253	0.6951	6.0496	0.7398	6.6360	0.7907	7.3044	0.8501	8.0913	0.9240	9.0654
	0.2	0.6524	5.4554	0.7092	6.2142	0.7751	7.0958	0.8538	8.1542	0.9555	9.5227	1.1160	11.6313
Channel	0	0.3152	1.0984	0.3152	1.0984	0.3152	1.0984	0.3152	1.0984	0.3152	1.0984	0.3152	1.0984
	0.0001	0.3152	1.0985	0.3152	1.0985	0.3152	1.0985	0.3152	1.0985	0.3152	1.0985	0.3152	1.0985
	0.001	0.3156	1.0992	0.3156	1.0992	0.3156	1.0992	0.3156	1.0992	0.3156	1.0992	0.3156	1.0992
	0.01	0.3198	1.1130	0.3199	1.1133	0.3200	1.1136	0.3200	1.1140	0.3201	1.1144	0.3202	1.1148
	0.02	0.3241	1.1337	0.3245	1.1359	0.3249	1.1383	0.3254	1.1409	0.3258	1.1434	0.3262	1.1461
	0.05	0.3338	1.1950	0.3364	1.2105	0.3391	1.2265	0.3419	1.2429	0.3447	1.2597	0.3476	1.2766
	0.1	0.3417	1.2740	0.3502	1.3277	0.3591	1.3839	0.3683	1.4422	0.3780	1.5027	0.3879	1.5655
	0.15	0.3436	1.3248	0.3590	1.4279	0.3751	1.5378	0.3920	1.6537	0.4096	1.7763	0.4280	1.9059
	0.2	0.3425	1.3549	0.3647	1.5129	0.3880	1.6821	0.4123	1.8636	0.4377	2.0565	0.4647	2.2658

Table 2: K_0 and K_1 for different C_2 and Kn .

		$C_2 = 0$		$C_2 = 0.1$		$C_2 = 0.2$		$C_2 = 0.3$		$C_2 = 0.4$		$C_2 = 0.5$	
Kn		K_0	K_1	K_0	K_1	K_0	K_1	K_0	K_1	K_0	K_1	K_0	K_1
Pipe	0.0001	76.3599	1.2655	76.3526	1.2655	76.3453	1.2655	76.3380	1.2655	76.3307	1.2655	76.3234	1.2655
	0.001	63.2900	1.2454	62.9725	1.2453	62.6644	1.2453	62.3652	1.2452	62.0746	1.2451	61.7920	1.2450
	0.01	31.4299	1.0866	29.5644	1.0850	28.2273	1.0835	27.1745	1.0822	26.3005	1.0810	25.5503	1.0798
	0.02	21.6288	0.9478	19.4039	0.9439	18.0081	0.9403	16.9569	0.9369	16.1016	0.9335	15.3752	0.9302
	0.05	10.9205	0.6591	8.5012	0.6449	7.1769	0.6312	6.2058	0.6176	5.4263	0.6043	4.7707	0.5911
	0.1	5.3864	0.4029	3.0287	0.3709	1.8488	0.3403	1.0098	0.3109	0.3544	0.2826	-0.1826	0.2554
	0.15	3.2671	0.2712	1.0311	0.2254	-0.0133	0.1831	-0.7275	0.1439	-1.2648	0.1075	-1.6889	0.0737
	0.2	2.2047	0.1948	0.0940	0.1391	-0.8284	0.0896	-1.4311	0.0456	-1.8646	0.0062	-2.1910	-0.0291
Channel	0.0001	80.3390	0.6802	80.3745	0.6912	80.3672	0.6912	80.3599	0.6912	80.3526	0.6912	80.3453	0.6912
	0.001	67.2768	0.6726	66.9628	0.6814	66.6541	0.6813	66.3544	0.6813	66.0632	0.6812	65.7801	0.6812
	0.01	35.1348	0.6086	33.2312	0.6110	31.8826	0.6101	30.8196	0.6093	29.9364	0.6086	29.1775	0.6079
	0.02	25.0101	0.5505	22.7359	0.5513	21.3181	0.5496	20.2478	0.5480	19.3757	0.5466	18.6339	0.5452
	0.05	13.5077	0.4184	11.0197	0.4147	9.6489	0.4088	8.6385	0.4030	7.8251	0.3974	7.1392	0.3918
	0.1	7.1224	0.2825	4.6717	0.2700	3.4163	0.2555	2.5153	0.2415	1.8063	0.2279	1.2214	0.2147
	0.15	4.5213	0.2055	2.1511	0.1823	1.0139	0.1606	0.2249	0.1401	-0.3764	0.1209	-0.8570	0.1028
	0.2	3.1242	0.1522	0.8822	0.1252	-0.1416	0.0984	-0.8240	0.0740	-1.3239	0.0519	-1.7076	0.0317

List of Figures

1	$u_{s,fd}^*$ and $u_{c,fd}^*$ for pipe and channel flows as functions of Kn for different C_2 .	14
2	Variations in $\Delta p_{m,\infty}^*$ as functions of Kn for pipe and channel flows.	17
3	Development of u/u_{av} as functions of r/R at different axial locations for pipe flows.	20
4	$L_{fd}^* = L_{fd}/D_h$ as functions of Re . The symbols represent the raw computational data and the lines are obtained according to Eq. (19).	22
5	Performance of the correlations for L_{fd}^* . The solid lines represent 100% accuracy.	25
6	Comparison of different correlations for L_{fd}^* for channel flows with $Kn = 0.2$ and $C_2 = 0$	27
7	Effects of Kn on variations in $K(x)$ as functions of x/D_h for pipe flows with $C_2 = 0$	28
8	Effects of Kn on variations in $K(x)$ as functions of x/D_h for pipe flows with $C_2 = 0.5$	29
9	Effects of C_2 on variations in $K(x)$ as functions of x/D_h for pipe flows with $Kn = 0.2$	30
10	Effects of C_2 on variations in $K(x)$ as functions of x/D_h for pipe flows with $Kn = 0.01$	31
11	Effects of C_2 on variations in $K(x)$ as functions of x/D_h for channel flows with $Kn = 0.2$	32
12	Effects of C_2 on variations in K_{fd} as functions of Re for Pipe flows with different Kn . The symbols represent the simulated data and the lines are obtained according to Eq. (24).	33
13	Effects of C_2 on variations in K_{fd} as functions of Re for Channel flows with different Kn . The symbols represent the simulated data and the lines are obtained according to Eq. (24).	35
14	Performance of correlations for K_{fd} . The solid lines represent 100 % accuracy.	37

List of Tables

1 L_0 and L_1 for different C_2 and Kn 50

2 K_0 and K_1 for different C_2 and Kn 51